# Self-Consistent Hartree-Fock Based Random Phase Approximation And The Spurious State Mixing

B. K. Agrawal<sup>1)</sup>, S. Shlomo<sup>1)</sup>, and A. I. Sanzhur<sup>1,2)</sup>

1) Cyclotron Institute, Texas A&M University, College Station, TX 77843-3366

2) Institute for Nuclear Research, Kiev 03028, Ukraine

# Abstract

We use a fully self-consistent Hartree—Fock (HF) based continuum random phase approximation (CRPA) to calculate strength functions S(E)and transition densities  $\rho_t(r)$  for isoscalar giant resonances with multipolarities L=0, 1 and 2 in  $^{80}Zr$  nucleus. In particular, we consider the effects of spurious state mixing (SSM) in the isoscalar giant dipole resonance (ISGDR) and extend the projection method to determine the mixing amplitude of spurious state so that properly normalized S(E)and  $\rho_t(r)$  having no contribution due to SSM can be obtained. For the calculation to be highly accurate we use a very fine radial mesh (0.04 fm)and zero smearing width in HF-CRPA calculations. We first use our most accurate results as a basis to establish the credibility of the projection method, employed to eliminate the SSM, and then to investigate the consequences of the common violation of self-consistency, in actual implementation of HF based CRPA and discretized RPA (DRPA), as often encountered in the published literature. The HF-DRPA calculations are carried out using a typical box size of 12 fm and a very large box of 72 fm, for different values of particle-hole energy cutoff ranging

from 50 to 600 MeV.

#### I. INTRODUCTION

Hartree-Fock (HF) based random phase approximation (RPA) has been a very successful theory in providing microscopic description of phenomena associated with collective motion in nuclei [1]. Accurate information for important physical quantities can be obtained by comparing the experimentally deduced strength function distribution, S(E), with the results obtained from HF-RPA theory. In particular, the strength function distributions of the isoscalar giant monopole resonance (ISGMR) and the isoscalar giant dipole resonance (ISGDR) are quite sensitive to the value of the nuclear matter incompressibility coefficient,  $K_{nm}$ , [1–4], a very important physical quantity since it is directly related to the curvature of the equation of state.

Over the last two decades, a significant amount of experimental work was carried out to identify the strength distributions of the isoscalar giant resonances in nuclei, particularly the ISGMR [3] and ISGDR [5]. The main development in the area of experimental investigation of the isoscalar giant resonances is the high accuracy data, of excitation cross section, by  $\alpha$ -particle scattering, obtained at Texas A&M University using a beam analysis system (BAS), a multipole-dipole-multipole (MDM) spectrometer and broad range multiwire proportional counter. The new system improved the signal to background ratio by more than a factor of 15. This led to the discovery of a high lying structure in the strength function of the ISGMR and the location of the ISGMR in light nuclei. Also, accurate data on the ISGDR has been obtained for a wide range of nuclei [5]. This has led to renewed interest in the nuclear response function and the need to carry out detailed and accurate calculations of S(E) and the transition density,  $\rho_t$ , within the HF-RPA theory. In particular there have been quite a few recent HF-RPA [6-10] and relativistic mean field (RMF) based RPA [11,12] calculations of the ISGDR, considering the issues of (i) spurious state mixing (SSM), (ii) the strength of the lower component (at  $1\hbar\omega$ ) and (iii) the value of  $K_{nm}$  deduced from the centroid energy  $E_1$  of the ISGDR compression mode (at  $3\hbar\omega$ ).

Comparison between the recent data on the ISGMR and the results of HF based

RPA calculations confirms the value of  $K_{nm} = 210 \pm 20$  MeV, determined earlier in [4]. It was first pointed out in Ref. [13] that the HF-RPA results for  $E_1$ , obtained with interactions adjusted to reproduce the ISGMR data, are higher than the experimental values [14,15] by more than 3 MeV and thus this discrepancy between theory and experiment raises doubts concerning the unambiguous extraction of  $K_{nm}$  from energies of compression modes. This discrepancy between theory and experiment was also reported in more recent experiments [5,16]. Recently, Shlomo and Sanzhur [9] have addressed this discrepancy by carrying out accurate microscopic calculations for S(E) and the excitation cross section  $\sigma(E)$  of the ISGDR, within the folding model (FM) distorted-wave-Born-approximation (DWBA), with  $\rho_t$  obtained from HF-RPA calculations and corrected for the SSM. They demonstrated that the calculated  $\sigma(E)$  drops below the experimental sensitivity in the region of high excitation energy containing 30-40% of the ISGDR energy weighted sum rule (EWSR). This missing strength leads to a reduction of more than 3.0 MeV in the value of  $E_1$  and thus explains the discrepancy between theory and experiment.

Clearly accurate calculations of S(E) and  $\sigma(E)$  are needed. In fully self-consistent HF-RPA calculations, the spurious isoscalar dipole (T=0, L=1) state (associated with the center of mass motion) appears at energy E=0 and no SSM in the ISGDR occurs. It was pointed out in [9] that none of the calculations carried out for S(E) and  $\rho_t$  and published in the literature are fully self-consistent. In some RPA calculations the mean field and the particle-hole interaction  $V_{ph}$  are chosen independently. Although this approach can provide physical insight on the structure of giant resonances, it can not be used to accurately determine important physical quantity such as  $K_{nm}$ . In self-consistent HF-RPA calculation [17] one starts by adopting specific effective nucleon-nucleon interaction,  $V_{12}$ , such as the Skyrme interaction, and carries out HF calculations. The parameters of the interaction are determined by a fit to properties of nuclei (binding energies, radii, etc.). Then one solves the RPA equation using the particle-hole (p-h) interaction  $V_{ph}$  which corresponds to  $V_{12}$ . However,

although not always stated in the literature, self-consistency is violated in actual implementations of the RPA (and relativistic RPA) calculations. One usually makes the following approximations: (i) use a  $V_{ph}$  which is not consistent with  $V_{12}$ . It is common to neglect the two-body Coulomb and spin-orbit interactions in  $V_{ph}$  and approximate the momentum dependent parts in  $V_{ph}$ , (ii) limiting the p-h space in a discretized calculation by a cut-off energy  $E_{ph}^{max}$ , and (iii) introducing a smearing parameter (i.e., a Lorentzian with  $\Gamma/2$ ). The consequences of these violations of self-consistency on S(E) and  $\rho_t$  and of numerical inaccuracy are usually ignored in the literature.

In this work we present results of detailed investigations of the consequences of common violations of self-consistency in actual implementations of HF based RPA, for determining the response functions S(E) and  $\rho_t$  of isoscalar multipole (L=0,1 and 2) giant resonances. In particular, we consider the ISGDR and concentrate on the effects of the SSM. We determine the effects of a violation of self-consistency by comparing the calculated results for S(E) and  $\rho_t$  with those obtained from highly accurate fully self-consistent HF- continuum RPA (HF-CRPA) calculations [18]. We also extend the projection method for eliminating the effects of SSM, described in Ref. [9], to properly normalize S(E) and  $\rho_t$  and determine the mixing amplitude of the spurious state in the ISGDR.

In Section II we present an extension of the Green's function based derivation of the projection operator method for eliminating the effects of the SSM, described in [9], to also account for the proper normalization of the S(E) and  $\rho_t(\mathbf{r})$  of the ISGDR and determine the mixing amplitude of the spurious state, obtained in HF-RPA calculations. We emphasize here that the method is quite general and applicable for any scattering operator F and for any numerical method used in carrying out the RPA calculation, such as configuration space RPA, coordinate space (continuum and discretized) RPA and with and without the addition of smearing. We also provide in this section the basic expressions used in the calculations and the presentation of our results.

In Section III we present and discuss our results. We first present the results of a highly accurate and fully self-consistent HF-CRPA calculation of S(E) and  $\rho_t(r)$  in  $^{80}Zr$ , which we use as a basis for a comparison with results obtained with common violations of self-consistency. These accurate fully self-consistent HF-CRPA results were obtained using  $\Gamma = 0$  (i.e., no smearing) and very small mesh sizes of  $dr_{HF} = 0.04$  fm and  $dr_{RPA} = 0.04$  fm with corresponding number of mesh points  $N_{HF} = 900$  and  $N_{RPA} = 300$ , used in the HF and the CRPA calculations, respectively. We note that the values of S(E) and  $\rho_t(r)$  associated with a bound RPA state were deduced from the residue of the RPA Green's function. Next, we present our results of fully self-consistent HF-CRPA calculations (with  $\Gamma = 0$ ) carried out using various mesh sizes  $dr_{HF}$  and  $dr_{RPA}$  and discuss the issue of numerical accuracy. We then present and discuss the results obtained with certain violations of self-consistency in CRPA and discretized RPA (DRPA) calculations and assess the effects on S(E)and  $\rho_t(E)$  by comparing with the highly accurate fully self-consistent results over the whole range of excitation energies. We point out that comparing the total energy weighted transition strength with the EWSR may lead to incorrect conclusions. Very recently the accuracy of the projection operator method in eliminating the effects of the SSM on S(E) and  $\rho_t$  of the ISGDR was investigated in Refs. [9,19]. However, in these works, the calculations carried out using mesh sizes  $dr \geq 0.1$  fm, were not fully self-consistent. We emphasize that in the present work we have carried out highly accurate self-consistent calculations, established the accuracy of the projection operator method and provide assessments on the effects on S(E),  $E_L$  and  $\rho_t$  of the isoscalar resonances with L=0, 1 and 2, which are due to common violation of selfconsistency in actual implementation of HF-RPA often encountered in the literature. We note that preliminary results of the present work were presented earlier [20]. In section IV we state our conclusion.

#### II. FORMALISM

The RPA Green's function G [17,18] is given by,

$$G = G_0(1 + V_{ph}G_0)^{-1} , (1)$$

where  $G_0$  is the free p-h Green's function given by,

$$G_0(\mathbf{r}, \mathbf{r}', E) = -\sum_h \phi_h(\mathbf{r}) \left[ \frac{1}{H_0 - \epsilon_h - \omega} + \frac{1}{H_0 - \epsilon_h + \omega} \right] \phi_h(\mathbf{r}'). \tag{2}$$

Here  $H_0$  is the HF hamiltonian and  $\epsilon_h$  and  $\psi_h$  are the single particle energy and the wave function of the occupied state, respectively. The continuum effects (particle escape width) are included by using

$$G_{lj}(\mathbf{r}, \mathbf{r}', E) = \frac{1}{H_0 - E} = -\frac{2m}{\hbar^2} u_{lj}(r_<) v_{lj}(r_>) / w,$$
 (3)

where  $r_{<}$  and  $r_{>}$  are the the lesser and the greater of r and r', respectively, u and v are the regular and irregular solution of  $H_0$ , with the appropriate boundary conditions, respectively and w is the Wronskian. The strength function S(E) and transition density  $\rho_t$ , associated with the scattering operator,

$$F = \sum_{i=1}^{A} f(\mathbf{r}_i) , \qquad (4)$$

are given by,

$$S(E) = \sum_{n} |\langle 0|F|n\rangle|^2 \,\delta(E - E_n) = \frac{1}{\pi} \text{Im} \left[\text{Tr}(fGf)\right],\tag{5}$$

$$\rho_t(\mathbf{r}, E) = \frac{\Delta E}{\sqrt{S(E)\Delta E}} \int f(\mathbf{r}') \left[ \frac{1}{\pi} \text{Im} G(\mathbf{r}', \mathbf{r}, E) \right] d\mathbf{r}' . \tag{6}$$

Note that  $\rho_t(\mathbf{r}, E)$ , as defined in (6), is associated with the strength in the region of  $E \pm \Delta E/2$  and is consistent with

$$S(E) = \left| \int \rho_t(\mathbf{r}, E) f(\mathbf{r}) d\mathbf{r} \right|^2 / \Delta E \quad . \tag{7}$$

It is important to note that S(E) and  $\rho_t$  of a state at energy  $E_n$  below the particle escape threshold (or having a very small width) can be obtained from Eqs. (5) and (6), respectively, by replacing  $\frac{1}{\pi} \text{Im} G(\mathbf{r}', \mathbf{r}, E)$  with

$$\lim_{E \to E_n} \operatorname{Re} G(\mathbf{r}', \mathbf{r}, E)(E - E_n), \tag{8}$$

The energy weighted sum rule (EWSR) associated with the operator  $f_{LM} = f(r)Y_{LM}$  is given by [1],

$$EWSR(fY_{LM}) = \int ES_{LM}(E)dE = \frac{\hbar^2}{2m} \frac{A}{4\pi} \left[ \langle 0| \left(\frac{df}{dr}\right)^2 + L(L+1) \left(\frac{f}{r}\right)^2 |0\rangle \right]. \quad (9)$$

Using the equation of continuity and assuming that there is only one collective state [23,24] with energy  $E_{coll}$ , exhausting 100% of the EWSR associated with the scattering operator  $f_{LM} = f(r)Y_{LM}$ , one obtains the form for the corresponding transition density,

$$\rho_t^{coll}(r) = -\frac{\hbar^2}{2m} \sqrt{\frac{2L+1}{EWSR(f_{LM})E_{coll}}} \left[ \left( \frac{1}{r} \frac{d^2}{dr^2} (rf) - \frac{L(L+1)}{r^2} f \right) \rho_0 + \frac{df}{dr} \frac{d\rho_0}{dr} \right]. \quad (10)$$

Let us consider scattering operators, Eq. (4), with

$$f(\mathbf{r}) = f(r)Y_{1M}(\Omega) , \quad f_1(\mathbf{r}) = rY_{1M}(\Omega) ,$$

$$(11)$$

and write  $\frac{1}{\pi} \text{Im} G$  as the sum of separable terms

$$R(\mathbf{r}', \mathbf{r}, E) = \frac{1}{\pi} \operatorname{Im} G(\mathbf{r}', \mathbf{r}, E) = \sum_{n} d_{n}(E) \rho_{n}(\mathbf{r}) \rho_{n}(\mathbf{r}') . \tag{12}$$

Note that  $d_n(E)$  accounts for the energy dependence of  $R(\mathbf{r}', \mathbf{r}, E)$ . In the case of a well defined resonance, or in a discretized continuum calculation, the sum in Eq. (12) has only one term. In this case  $\rho_n$  is proportional to the transition density associated with the resonance and may contain a spurious state contribution. In general, due to the smearing with  $\Gamma/2$ , the sum in Eq. (12) may contain quite a few terms. We now write  $\rho_n$  as

$$\rho_n(\mathbf{r}) = a_n \rho_{n3}(\mathbf{r}) + b_n \rho_{n1}(\mathbf{r}) , \qquad (13)$$

with

$$a_n^2 + b_n^2 = 1.0. (14)$$

Note that  $\rho_{n1}(\mathbf{r})$  is due to SSM and  $\rho_{n3}$ , associated with the ISGDR, fulfills the center of mass condition (for all n)

$$\langle f_1 \rho_{n3} \rangle = \int f_1(\mathbf{r}) \rho_{n3}(\mathbf{r}) d\mathbf{r} = 0 .$$
 (15)

We point out that in the projection method for eliminating the effects of SSM, described in Ref. [9], it was assumed that  $a_n = 1.0$  (in (13)).

Following the derivation described in Ref. [9], we first note that all  $\rho_{n1}$  coincide with the coherent spurious state transition density  $\rho_{ss}(\mathbf{r})$  [21]

$$\rho_{n1}(\mathbf{r}) = \rho_{ss}(\mathbf{r}) = -\sqrt{\frac{\hbar^2}{2m} \frac{4\pi}{AE_{ss}}} \frac{\partial \rho_0}{\partial r} Y_{1M}(\Omega) , \qquad (16)$$

where  $E_{ss}$  is the spurious state energy and  $\rho_0$  is the ground state density of the nucleus. Note that  $\rho_{ss}$  in (16) is normalized to 100% of the energy weighted sum rule (see (9) and (10)),

$$EWSR(rY_{1M}) = \frac{\hbar^2}{2m} \frac{3}{4\pi} A. \tag{17}$$

Looking for a projection operator that projects out  $\rho_{n1}(\mathbf{r})$ ,

$$F_{\eta} = \sum_{i=1}^{A} f_{\eta}(\mathbf{r}_{i}) = F - \eta F_{1} , \qquad (18)$$

with  $f_{\eta} = f - \eta f_1$ , we find that the value of  $\eta$  associated with  $\rho_{ss}$  is given by

$$\eta = \langle f \rho_{ss} \rangle / \langle f_1 \rho_{ss} \rangle. \tag{19}$$

Using (15) and (19) we have

$$S_{\eta}(E) = \langle f_{\eta} R f_{\eta} \rangle = \langle f R_{33} f \rangle, \tag{20}$$

where,

$$R_{33} = \sum d_n(E) a_n^2 \rho_{n3}(\mathbf{r}) \rho_{n3}(\mathbf{r}'). \tag{21}$$

To determine  $\rho_t$  for the ISGDR we first use (6), (12), (13), (15) and (19) with  $F_{\eta}$  and obtain

$$\rho_{\eta}(\mathbf{r}) = \frac{\Delta E}{\sqrt{S_{\eta}(E)\Delta E}} \sum c_n a_n [a_n \rho_{a3}(\mathbf{r}) + b_n \rho_{ss}(\mathbf{r})] , \qquad (22)$$

with  $c_n = d_n(E)\langle f_{\eta}\rho_{n3}\rangle$ . To project out the spurious term from (22) we make use of (15) and obtain

$$\rho_t(\mathbf{r}) = \rho_\eta(\mathbf{r}) - b\rho_{ss} , \quad b = \langle f_1 \rho_\eta \rangle / \langle f_1 \rho_{ss} \rangle .$$
(23)

To properly normalize  $S_{\eta}(E)$  and  $\rho_t$ , we have to determine the mixing amplitudes  $b_n$  of the spurious state in the ISGDR. These amplitude can be obtained from the response function to the scattering operator  $f_1$ . Using (13), (15) and (16) we obtained from (12),

$$S_1(E) = \langle f_1 R f_1 \rangle = \langle f_1 R_{11} f_1 \rangle = \sum_{n} d_n(E) b_n^2 \langle f_1 \rho_{ss} \rangle^2.$$
 (24)

Note that  $\langle f_1 \rho_{ss} \rangle$  can be obtained from the EWSR, Eq. (17),

$$\langle f_1 \rho_{ss} \rangle^2 = \hbar^2 2m \frac{3}{4\pi} A / E_{ss}, \tag{25}$$

and the SSM probabilities from

$$b_n^2 = \frac{S_1(E_n)}{\langle f_1 \rho_{ss} \rangle^2}.$$
 (26)

In the present work we limit our discussion to the operator  $F_3 = \sum_{i=1}^{A} f_3(\mathbf{r}_i)$ , where  $f(\mathbf{r}) = f_3(\mathbf{r}) = r^3 Y_{1M}(\Omega)$ . For this operator, the value of  $\eta$  associated with the spurious transition density (16) is

$$\eta = \frac{5}{3} \langle r^2 \rangle \ , \tag{27}$$

and

$$S_{\eta}(E) = S_3(E) - 2\eta S_{13}(E) + \eta^2 S_1(E), \tag{28}$$

where  $S_3(E) = \langle f_3 R f_3 \rangle$  is the strength function associated with  $f_3$  and  $S_{13} = \langle f_1 R f_3 \rangle$  is the non-diagonal strength function.

#### III. RESULTS AND DISCUSSIONS

In the following, we present our results for isoscalar giant resonances (L = 0, 1 and 2) obtained within the HF based RPA framework as briefly outlined in the previous section. Calculations are performed for  $^{80}Zr$  (N = Z = 40). The two-body interaction  $V_{12}$  is taken to be of a simplified Skyrme type,

$$V_{12} = \delta(\vec{r}_1 - \vec{r}_2) \left[ t_0 + \frac{1}{6} t_3 \rho^{\alpha} \left( \frac{\vec{r}_1 + \vec{r}_2}{2} \right) \right], \tag{29}$$

where  $\alpha = 1/3$ ,  $t_0 = -1800 \text{ MeVfm}^3$  and  $t_3 = 12871 \text{ MeVfm}^{3(\alpha+1)}$ . For these values of the interaction parameters the nuclear matter equation of state has a minimum at E/A = -15.99 MeV,  $\rho_0 = 0.157 \text{ fm}^{-3}$  with  $K_{nm} = 226 \text{ MeV}$ , where E/A,  $\rho_0$  and  $K_{nm}$  being the binding energy per nucleon, matter saturation density and incompressibility coefficient for symmetric nuclear matter, respectively. This choice of the two-body interaction enables us to use the continuum RPA method to carry out a fully self-consistent calculation for giant resonances. Following Ref. [22] one can write the mean field potential  $V_{mf}$  as,

$$V_{mf} = \frac{3}{4}t_0\rho(r) + \frac{\alpha+2}{16}t_3\rho^{\alpha+1}(r)$$
(30)

and the particle-hole interaction  $V_{ph}$  contributing to the isoscalar channel is given by [17]

$$V_{ph} = \delta(\vec{r}_1 - \vec{r}_2) \left[ \frac{3}{4} t_0 + \frac{(\alpha + 1)(\alpha + 2)}{16} t_3 \rho^{\alpha} \right]. \tag{31}$$

To begin with, we consider our results for isoscalar giant monopole, dipole and quadrupole resonances which are fully self-consistent and numerically accurate. Then, we shall analyze the influence of various numerical approximations on the centroid energies and transition densities for these resonances. Finally, we shall illustrate the possible effects of the violation of self-consistency on the properties of these isoscalar giant resonances (ISGR).

#### A. Self-consistent continuum RPA results

We now present our results of fully self-consistent HF-CRPA calculations for  $^{80}Zr$ , using the Skyrme interaction of Eq. (29) with spin-orbit and Coulomb interactions switched off. It was pointed out in [18] that in order to have cancellations of the hole-hole transitions occurring in  $G_0$  (Eq. (2)) and obtain numerically accurate results, it is important to employ the same mean-field and the same integration algorithm for the bound states and the single-particle Green's function, using a small mesh size in double precision calculations. In the following we first present our results of highly accurate calculations obtained using  $dr_{HF} = 0.04$  fm and  $dr_{RPA} = 0.04$  fm, and with no smearing ( $\Gamma = 0$  MeV), which we use in the following as a basis for comparison with other calculations. We note that in common implementations of HF-RPA one usually adopts the values of  $(dr_{HF}, dr_{RPA})$ =(0.1 fm, 0.3 fm) and a smearing parameter of  $\Gamma/2 \sim 1.0$  MeV. In the following we use the notation  $dr = (dr_{HF}, dr_{RPA})$ , with the values given in units of fm.

To facilitate our discussions we have displayed in Table I the HF single-particle energies for  $^{80}Zr$  obtained for  $dr_{HF}=0.04$  fm. In Table II we give the values for the density radial moments  $\langle r^2 \rangle$ ,  $\langle r^4 \rangle$  and EWSRs (Eq. (9)) for various multipoles evaluated for different values of mesh size in the HF calculation. In Table III we present the values of energy weighted transition strengths (EWTS) for free and CRPA responses obtained using the operators  $f_3$ ,  $f_1$  and  $f_\eta$  with dr=(0.04,0.04) and  $\Gamma=0$  MeV. The quantities  $S_1^{EW}$ ,  $S_3^{EW}$ ,  $S_{13}^{EW}$  and  $S_{\eta}^{EW}$  in Table III denote the EWTS for the corresponding strength functions  $S_1$ ,  $S_3$ ,  $S_{13}$  and  $S_{\eta}$ , respectively, see Eq. (28). The transition strengths associated with sharp transitions were determined from the residues of the Green's function, using its real part (see Eq. (8)). For the free response we get sharp peaks at the bound state single particle-hole transitions associated with L=1. These transitions can be easily identified from Table I as  $0g \to 0f$  (10.83),  $1d \to 1p$  (11.35),  $2s \to 1p$  (12.70),  $1d \to 0f$  (17.43),  $1d \to 0p$  (35.16), and  $2s \to 0p$  (36.52), with corresponding transition energies given in brackets in MeV. We checked

that the values of the EWTS for these sharp transitions agree with the corresponding values obtained directly from the particle and hole wave functions.

For CRPA response, the sharp peaks occur below the particle threshold at 15.33 MeV. In addition to these sharp transitions, we have contributions from the continuum starting at the particle threshold. We obtained the contributions from the continuum by integrating the energy weighted strength function using small enough energy steps of dE = 0.01 MeV. It is seen from Table III that the spurious state mixing is significantly larger for the free response (see 3rd column). Once the spurious state mixing is eliminated using the projection operator  $f_{\eta}$  we find from the 2nd and 5th columns of this table that most of the strengths of the free response in the  $1\hbar\omega$ region of excitation energy (E < 20 MeV) is spurious in nature. Only 6.8% of the EWTS for the operator  $f_3$  contributes to the intrinsic excitations for E < 20 MeV. On the other hand, in the case of CRPA, since the calculation is fully self-consistent and numerically very accurate, the resonance occurring at 0.079 MeV is fully spurious and it exhausts 99.99% of the EWSR associated with the operator  $f_1$ . For E > 0.08MeV, the values of  $S_1$  and  $S_{13}$  are so small that SSM is negligible. We see from the Table III that the values of  $b_n^2$  is  $\sim 10^{-8}$  (see Eq.( 26)) indicating that the SSM is so small that one need not renormalize the strength  $S_{\eta}$ . For E > 0.08 MeV, the values of the CRPA EWTS for the operators  $f_3$  and  $f_{\eta}$  are the same within 1%. We would like to emphasize that though the spurious state mixing is significantly large for the free response, it is fully eliminated by using the projection operator  $f_{\eta}$  giving rise to 99.95% of the expected EWSR which is quite close to the CRPA results. It may also be added that the fraction energy weighted sum rule, FEWSR = EWTS/EWSR, for the operator  $f_{\eta}$  is 8.4% and 7.4% for E < 20 MeV in the case of free and CRPA responses, respectively.

A proper test of a fully self-consistent calculation is to check how close  $\rho_t(r, E_{ss})$  is to  $\rho_{ss}$ , where  $\rho_t(r, E_{ss})$  is obtained from Eqs. (6) and (8) at the spurious state energy  $E_{ss}$  using  $f_1$ . In Fig. 1 we compare the CRPA result for the  $\rho_t(r, E_{ss})$  with

the coherent state transition density calculated using Eq. (16). It is seen in Fig. 1 that in this highly accurate HF-CRPA calculation  $\rho_t(r, E_{ss})$  coincides with  $\rho_{ss}$ , indicating a very negligible SSM.

We shall now present some plots for the strength functions for various multipoles obtained from our most accurate calculations. For plotting purpose we used a very small smearing width  $\Gamma/2 = 0.025$  MeV. In Figs. 2 and 3 we have shown the free and RPA response for the ISGDR, respectively. We see from Fig. 2 that most of the spurious components lie in the low energy region (E < 20 MeV). As mentioned before, we see that the response for the operators  $r^3$  and  $(r^3 - \eta r)$  are indistinguishable in the case of a fully self-consistent HF based CRPA calculation. It also appears from these figures that particle-hole correlations do not alter the ISGDR strength distribution (shown in Fig. 2) very much which suggests that the isoscalar dipole state is not a very collective one. In Figs. 4 and 5 we have shown the plots for the ISGMR and ISGQR response functions, respectively. We have also carried out these calculations for dr = (0.24, 0.24) (not shown here) and find that they can not be distinguished from our most accurate calculations. We also note that at the surface the transition density for ISGMR looks like  $3\rho_0 + rd\rho_0/dr$  as given by Eq. (10), whereas, the ISGQR transition density looks more like  $d\rho_0/dr$  rather than  $rd\rho_0/dr$  as given by Eq. (10). We point out that Eq. (10) was derived under the assumption that one collective state exhausts the EWSR.

We have repeated the fully self-consistent calculations for  $\Gamma=0$  MeV, using various values of  $dr_{HF}$  and  $dr_{RPA}$ . In Table IV we present CRPA results for the EWTS only for dr=(0.24,0.24) and (0.04,0.24) with  $N_{RPA}=50$ . We see from Table IV that the results for the operator  $f_3$  for the different combinations of the mesh size differ by about 2.5%. The spurious state for dr=(0.24,0.24) occurs at 0.7 MeV and its excitation energy becomes imaginary for dr=(0.04,0.24). By multiplying the particle-hole interaction by a constant factor  $V_{sc}=0.9916$  we push the spurious state to 0.1 MeV for dr=(0.04,0.24) calculations. Nevertheless, we find that the SSM, or

equivalently  $b_n^2$  is very small ( $\sim 10^{-6}$ ). Once the spurious components are eliminated using the projection operator  $f_{\eta}$ , we get 99.40% and 99.76% of the expected EWSR for dr = (0.24, 0.24) and (0.04, 0.24), respectively. So far we have demonstrated that (i) as long as the calculation is fully self-consistent and numerically highly accurate, there is practically no spurious state mixing and (ii) the spurious state mixing introduced due to the use of a large mesh size (0.24 fm) in a CRPA calculation can be projected out using the operator  $f_{\eta}$ .

In Tables V and VI we have collected the centroid energies and the FEWSR, respectively, for the isoscalar resonances with L=0, 1 and 2 calculated using different combinations of the mesh size and a fixed value of  $\Gamma/2=0.025$  MeV. We notice that as long as the particle-hole interaction is not renormalized (i.e.,  $V_{sc}=1.0$ ) the centroid energies of the resonances do not deviate by more than 0.5% compared with the most accurate values. Though the energy of spurious state is sensitive to the values of the mesh sizes and increases from 0.08 MeV to 0.71 MeV with the increase of radial mesh size from 0.04 fm to 0.24 fm, the centroid energy for ISGDR changes only by about 0.08 MeV. Even if  $V_{sc}$  is used to shift the spurious peak to 2.0 MeV, the centroid energy for L=0 and L=1 resonance do not change appreciably. However, the centroid energy for the L=2 resonance goes up by about 2% (0.3 MeV). It is also clear from Table V and Figs. 3, 4 and 5 that the peak energy for ISGMR and ISGDR is higher than their centroid energies by about 0.5 and 0.15 MeV, respectively. From the Table VI we find that when dr=(0.04,0.24), the values of the total EWTS for ISGMR and ISGQR are overestimated by 1-2%.

#### B. Influence of the smearing parameter $\Gamma$

One of the requirements to avoid any SSM is that one must not use any smearing parameter (i.e.,  $\Gamma=0$ ) and the calculations should be performed using a very fine mesh in the co-ordinate space while solving HF and RPA equations. However, one typically uses  $\Gamma/2 \sim 1.0$  MeV and the mesh  $dr \geq 0.1$  fm. If the smearing width is

finite, the spurious state would have a long energy tail which can give rise to large SSM. Because,  $\rho_{ss} \propto d\rho_0/dr$ , which is a surface peaked functions, and has a large matrix element for the operator  $f_3$ . One must project out the SSM by making use of the projection operator  $f_{\eta}$ .

In Fig. 6 we plot CRPA results for the spurious state and ISGDR strength functions calculated using radial mesh size of 0.04 fm and smearing parameter  $\Gamma/2 = 1$ MeV. We clearly see from the figure that the strength function for the spurious state is extended up to a very high energy. The SSM caused due to the energy tail of the spurious state is eliminated using the operator  $f_{\eta}$ . In Table VII we give the values of FEWSR, associated with the scattering operator  $f_{\eta}$ , for the ISGDR for various energy ranges up to 150 MeV obtained using different values for the mesh size and the smearing parameter in the HF-CRPA calculation. Considering the values of the FEWSR in each energy range  $\omega_1 - \omega_2$  of Table VII it can be easily seen that these values are practically the same as those obtained with  $\Gamma = 0$ , i.e., the SSM due to non-zero  $\Gamma$  is completely projected out. For  $\Gamma/2 = 1.0$  MeV the values for FEWSR for E=0-18 MeV is lower by about 1% as compared to that for  $\Gamma=0$ . This is because of the resonance at  $\sim 17.0 \text{ MeV}$  (see Fig. 3). If we integrate the energy weighted strength for E = 0-20 MeV, this difference reduces from 1% to about 0.5%. We also note that for  $\Gamma/2 = 1.0$  MeV the total FEWSR obtained by integrating up to E = 150 MeV is about 1% lower than the one obtained for  $\Gamma = 0$ . Of course, this is because of the remaining strength beyond 150 MeV. For instance, in the case of dr = (0.24, 0.24) and  $\Gamma/2 = 1.0$  MeV we get FEWSR = 0.48% for the region for E = 150 - 300 MeV.

We point out that due to  $\Gamma \neq 0$ , the transition density  $\rho_t$  calculated using Eq. (6) depends on the scattering operator f. The consequences of this on the S(E) and  $\rho_t$  of the ISGDR was investigated and discussed in detail in Ref. [9] and we do not repeat it here. We thus demonstrated that using the projection scattering operator  $f_{\eta}$  one can accurately eliminate the SSM effects occurring due to the use of a finite

smearing parameter  $\Gamma/2$ .

#### C. HF-DRPA results

The continuum can be discretized by confining the nucleus in a box of finite size. One can satisfactorily reproduce the continuum results, provided the calculations are carried out using a box of very large size (i.e., dense discretization) and the cut-off for the particle-hole excitation energy  $(E_{ph}^{max})$  set to be reasonably high. We now consider our results obtained by discretizing the continuum using boxes of different sizes. The length of the box is given by  $N_{HF}$  times  $dr_{HF}$ , where  $N_{HF}$  is the number of radial mesh point used in a HF calculation. In the following, we present the results for discretized RPA calculations obtained using dr = (0.08, 0.24) with  $N_{HF} = 150$  and 900 (box sizes of 12 and 72 fm, respectively). In Figs. 7a, and 7b we show the ISGDR response for box sizes of 12 and 72 fm and smearing parameter  $\Gamma/2 = 0.25$  and 1.0 MeV, keeping  $E_{ph}^{max} = 200$  MeV, together with the corresponding results obtained in HF-CRPA. We see that the DRPA results obtained for the larger box coincide with the results obtained within CRPA. The transition strength gets fragmented if the discretization is carried out using a small box. To avoid misleading interpretation of the fragmentation and obtain agreement with the CRPA results, one needs to use a larger value of the smearing parameter, consistent with the size of the box. To examine more closely the effects of discretization on the response function we present in Table VIII our DRPA results for the FEWSR over various energy ranges up to 150 MeV. It is evident from this table that the total FEWSR increases significantly when  $E_{ph}^{max}$  is increased from 50 MeV to 200 MeV. This increase is about 5-6% and 9-10% for  $\Gamma=0.5$  and 2 MeV, respectively. With a further increase in  $E_{ph}^{max}$  there is no noticeable change in the value of the total FEWSR. It can be easily verified from this table that the FEWSR associated with the low-lying ISGDR component (E < 20MeV) increases from 6.4% to 6.9% when  $E_{ph}^{max}$  is increased from 50 to 200 MeV for the case of  $N_{HF} = 150$  and  $\Gamma = 0.5$  MeV and it further increases to 7.2% for  $N_{HF} = 900$  (see also Table VII). Comparing the Tables VII and VIII we can conclude (see also Figs. 7a and 7b) that with the proper choice of discretization and  $E_{ph}^{max}$  one can mimic the continuum even for smaller values of  $\Gamma \sim 0.5 - 1.0$  MeV. Comparing the values of FEWSR, in each of the energy range  $\omega_1 - \omega_2$ , of Table VIII with Table VII we conclude that using  $f_{\eta}$  one accurately eliminates SSM occurring due to the use of a low value for  $E_{ph}^{max}$ .

In Table IX we have displayed the values of  $E_{ss}$  and the centroid energies for the L=0, 1 and 2 isoscalar giant resonances. These results are obtained using  $N_{HF}=900, \Gamma/2=0.25$  MeV with different values of  $E_{ph}^{max}$  in HF-DRPA calculations. The corresponding HF-CRPA results are given in the last row of the table. We clearly see that as  $E_{ph}^{max}$  increases, the centroid energies  $E_0$ ,  $E_1$  and  $E_2$  converge to their corresponding exact values obtained using HF-CRPA. However, this convergence is slower for the spurious state energy  $E_{ss}$ . For low values of  $E_{ph}^{max}$  we observe that the centroid energy for ISGMR is overestimated by 0.5 MeV, which can significantly effect the value of nuclear incompressibility. We also notice that  $E_1=35.3$  MeV is little low for  $E_{ph}^{max}=50$  MeV, because of the fact that the resonance energy for the ISGDR compressional mode is about 35.5 MeV (see also Fig. 3).

We saw in the previous subsection that the spurious transition density  $\rho_t(r, E_{ss})$  obtained using a fully self-consistent CRPA calculation is indistinguishable from the corresponding collective model form for  $\rho_{ss}$  which is proportional to  $d\rho_0/dr$ . In Fig. 8 we show some of the DRPA results for  $\rho_t(r, E_{ss})$  and compare them with the  $\rho_{ss}$ . We see that for  $E_{ph}^{max} = 50$  MeV  $\rho_t(r, E_{ss})$  deviates from  $d\rho_0/dr$  even for the case of  $N_{HF} = 900$ . However, for  $E_{ph}^{max} = 200$  MeV, the  $\rho_t(r, E_{ss})$  from the DRPA is almost identical to the collective model results. Thus, one must use a reasonably large value for the cut-off energy,  $E_{ph}^{max}$ , in order to fully eliminate from the intrinsic excitations the contribution due to SSM.

#### D. Effects of violation of self-consistency

So far we have examined the various effects of numerical approximation on the properties of the isoscalar giant resonances of multipolarity L = 0 - 2 and established the validity of the projection operator method in eliminating the SSM effects from the ISGDR. Here we report our investigations of the influence of certain violations of self-consistency on the strength function for isoscalar giant monopole (L=0), dipole (L=1) and quadrupole (L=2) resonances. These investigations are quite important in view of the fact that one often performs non self-consistent calculations for giant resonances such as the use of a phenomenological nuclear mean field (e.g., Woods-Saxon potential) and Landau-Migdal particle-hole interaction [8]. Moreover, one often come across HF-RPA calculations carried out using particle-hole interaction not consistent with the mean field used in HF. We present below the results for HF based CRPA calculations carried out with the two-body interaction given in Eq. (29). We use the parameter  $V_{sc}$  to renormalize the particle-hole interaction (i.e.,  $t_0 \to t_0 V_{sc}$ and  $t_3 \to t_3 V_{sc}$  in Eq. (31)) so that the position of the spurious state can be adjusted close to zero. To study the consequences of the violation of self-consistency we vary  $t_0$  and  $t_3$  only in the particle-hole interaction (only in Eq. (31)).

In Table X we summarize our results for the centroid energies for isoscalar giant resonances for L=0-2. The quantity  $K'_{nm}$  is the nuclear matter incompressibility coefficient associated with the renormalized parameters  $t_0V_{sc}$  and  $t_3V_{sc}$ . Here,  $t_0$  and  $t_3$  are the values used in Eq. (31). Let us first consider the results obtained by varying  $t_0$  by  $\pm 5\%$  and  $\pm 10\%$  and keeping  $t_3=12871$  MeVfm<sup>4</sup>. It can be clearly seen from the table that the centroid energies for ISGMR and ISGDR significantly differ from their corresponding self-consistent values even if  $V_{sc}$  is adjusted to give  $E_{ss}=0.1$  MeV. On the other hand, the centroid energy for ISGQR reattains its self-consistent value when  $V_{sc}$  is adjusted to yield  $E_{ss}=0.1$  MeV. One may understand this discrepancy in terms of the incompressibility coefficient. With the renormalization of  $V_{ph}$ , though,  $E_{ss}$  becomes close to zero, but values of  $K'_{nm}$  in the RPA calculation remain quite

different then the HF value of 226 MeV. In Fig. 9 we plot the values of  $E_0$  and  $E_1$  versus  $\sqrt{K'_{nm}}$  for the cases with  $E_{ss}=0.1$  MeV. This plot clearly depicts the systematic increase in  $E_0$  and  $E_1$  with increase in  $K'_{nm}$ . One may be tempted to infer at this point that as long as the nuclear matter incompressibility associated with the particle-hole interaction and the mean field is the same, centroid energies for the resonances considered here may come out to be reliable. In order to verify this, we adjust  $t_3$  in particle-hole interaction in such a way that  $K'_{nm}$  becomes 226 MeV when  $t_0$  is varied by  $\pm 10\%$ . We see from Table X that even if  $K'_{nm}$  is adjusted to 226 MeV, the values of  $E_0$  and  $E_1$  are off by about 10% and 3.5%, respectively. This is due to the fact that the shape of the particle-hole interaction is not the same, though, the  $K'_{nm}$  is kept constant. We note that if the ISGMR centroid energy is determined within 10% accuracy, the value of nuclear matter incompressibility will be correct only within 20%.

Apart from the centroid energies for the giant resonances, it is also important to investigate the effects on the strength function itself when the self-consistency is not maintained. We looked into the plots for the strength functions S and  $S_{\eta}$  for the operators  $f_3$  and  $f_{\eta}$ , respectively, for the different cases listed in Table X. We find that  $S_3 \geq S_{\eta}$  or  $S_3 < S_{\eta}$ , depending on the sign of interference between the spurious state and the intrinsic state (i.e., sign of the non-diagonal strength  $S_{13}$ ). As an illustrative example, we show in Fig. 10 our results for the case in which  $t_0$  is varied by -10% and  $V_{sc} = 1.7118$ . Similar is the case when  $t_0$  is varied by -5% and  $V_{sc} = 1.2938$ . These values of  $V_{sc}$  were chosen so that  $E_{ss} = 0.1$  MeV. In Figs. 11a, 11b and 11c we compare the fully self-consistent results for isoscalar giant resonances with those obtained by varying  $t_0$  by  $\pm 5\%$  in Eq. (31) and  $V_{sc}$  is adjusted to yield  $E_{ss} = 0.1$  MeV. We see that the strength function for ISGMR and ISGDR are significantly different compared with their corresponding self-consistent results. Whereas, in case of ISGQR not only their centroid energies, but also the strength function seem to agree well with the corresponding self-consistent results. It is very important to

point out that the violation of self-consistency causes redistribution of the strength in such a way that the total EWTS remains unaltered. This redistribution may be crucial in determining the energy weighted strengths associated with the low energy and the high-lying energy components of the ISGDR. For example, the fraction of the EWSR (in percent) for the energy range E = 0 - 20 MeV is 6.94, 9.33 and 12.42 for  $t_0 = -1710$ , -1800 and -1890 MeV fm<sup>3</sup>, respectively, and for E = 0 - 150 MeV we have for the FEWSR = 99.76% in these three cases.

We now focus on the influence of self-consistency violation when the continuum is discretized. As seen above, the discretization introduces two additional constraints, namely, the box size used in HF calculations and the maximum allowed particle-hole energy  $E_{ph}^{max}$ . We present here only the results for box size of 12 fm with  $E_{ph}^{max} = 50$ and 200 MeV. In Fig. 12 we compare the ISGDR response function obtained for  $t_0 = -1620$ , -1800 and -1980 MeVfm<sup>3</sup>, keeping  $E_{ph}^{max} = 50$  MeV. Similar results are shown in Fig. 13 but obtained by raising  $E_{ph}^{max}$  to 200 MeV. From  $S_3(E)$  we see clearly that when the particle-hole interaction is in accordance with the mean-field potential, the SSM is only due to  $\Gamma \neq 0$ . For the cases with  $t_0 \neq -1800 \text{ MeV fm}^3$ one can immediately see a marked enhancement in spuriocity at E = 10 - 12 MeV. Furthermore, it is startling to see that the total FEWSR associated with operator  $f_{\eta}$  for  $t_0=-1620$  and -1980 MeVfm<sup>3</sup> is 94.97% and 58.97%, respectively, and it is 95.13 % for  $t_0 = -1800~{\rm MeV fm^3}$ . For  $t_0 = -1710~{\rm MeV fm^3}$  we get a total FEWSR = 88.39% which is once again too much off compared to its expected value. We repeated the same analysis for box size 72 fm keeping  $E_{ph}^{max} = 50$  MeV but did not find any appreciable change in the values of the total FEWSR. However, when we raised the  $E_{ph}^{max}$  from 50 to 200 MeV, we get the total FEWSR 99.63%, 100.52% and 99.94% for  $t_0 = -1620$ , -1800 and -1980 MeVfm<sup>3</sup>, respectively.

We also calculate the SSM probabilities (i.e.,  $b_n^2$ ) when self-consistency is not maintained. The values of  $b_n^2$  are extracted using an extremely small smearing parameter. In case of  $t_0 = -1620 \text{ MeVfm}^3$  and  $E_{ph}^{max} = 50 \text{ MeV}$  used in DRPA calculation, we

find that  $E_{ss} = 9.84$  MeV. We get from Eq. (26),  $b_n^2 = 2.4\%$  for the state occurring at  $\sim 13$  MeV. When  $V_{sc}$  is adjusted to push the spurious state energy  $E_{ss}$  to about 0.1 MeV, the EWTS of the 13 MeV state, associated with SSM, remains unchanged. Consequently  $b_n^2$  reduces by two orders of magnitude. We thus conclude that since the values of  $b_n^2$  are less than a few percent even with large violation of self-consistency, the renormalization of the strength function is not needed.

We have considered the effects on the ISGDR strength function when Coulomb/spin-orbit interaction is switched on in the HF calculation, but, ignoring it in the particle-hole interaction. We find that when spin-orbit interaction is included, the strength function obtained using  $\Gamma/2 = 1$  MeV hardly gets affected at any energy and the differences can not be seen on the plots (not shown here). This is due to the fact that the nucleus in question,  $^{80}Zr$ , is spin saturated, i.e., the single-particle states with  $j = l \pm 1/2$  are occupied. However, this may not be the case for non spin-saturated heavy nuclei. When we carried out similar exercise with the Coulomb interaction, the mean field changes significantly and we find that the strength functions gets shifted towards lower energy by about 2.0 MeV. We note that, with the inclusion of Coulomb interaction, the particle threshold for protons reduces from 15.33 MeV to 3.5 MeV.

#### IV. CONCLUSIONS

We have carried out self-consistent HF based CRPA calculations for isoscalar giant resonances with multipolarities L=0, 1 and 2 for  $^{80}Zr$  nucleus as an example. We demonstrate that if a self-consistent calculation is performed using zero smearing width and a very fine radial mesh size (dr=0.04 fm), the spurious state occurs at  $E_{ss}=0.08 \text{ MeV}$  and the ISGDR response for the operators  $f_3$  and  $f_\eta$  are essentially the same for the energy  $E>E_{ss}$  which indicates no SSM and the corresponding EWSR is reproduced remarkably well. When we use dr=0.24 fm in HF and CRPA calculations,  $E_{ss}$  becomes about 0.7 MeV and there exists a small SSM. The amplitude

of this SSM (i.e.,  $b_n^2$ ) is  $\sim 10^{-6}$ , which is negligibly small and one need not renormalize the projected strength function. Although the position of the spurious state is quite sensitive to the radial mesh size and smearing parameter  $\Gamma$ , the centroid energy for the isoscalar resonances for L=0, 1 and 2 do not change by more than 0.5%.

We have also performed the calculation for L=0, 1 and 2 isoscalar resonances by discretizing the continuum using boxes of different sizes (12 and 72 fm) with  $E_{ph}^{max}$ ranging from 50-600 MeV. We found that the strength distribution is fragmented over a wide energy range for the case of the smaller box irrespective of  $E_{ph}^{max}$ . For the case of discretization in a large box (72 fm) with  $E_{ph}^{max} = 200$  MeV we find that the strength distribution agrees reasonably well with the corresponding one obtained from CRPA, if a moderate value of the smearing parameter ( $\Gamma/2 \sim 1$  MeV) is used. The spurious state occurs at about 4.5 MeV for  $E_{ph}^{max} = 50$  MeV for both the small as well as large box discretization considered. With the increase of  $E_{ph}^{max}$  to 600 MeV, we find that  $E_{ss}$  approaches the corresponding value obtained within the CRPA. The centroid energies for L=0, 1 and 2 resonances converge to their corresponding exact values obtained from HF-CRPA. This convergence is little slow in case of spurious state energy. For  $E_{ph}^{max} = 50$  MeV, the transition density  $\rho_t(r, E_{ss})$  at the spurious state energy obtained using discretized RPA differs from the corresponding CRPA results (which reproduce  $\rho_{ss}$ ). However, with increase of  $E_{ph}^{max}$  to 200 MeV, DRPA results for the spurious state transition density  $\rho_t(r, E_{ss})$  become quite close to the CRPA results. We also point out that one should use  $E_{ph}^{max} \geq 200$  MeV in order to calculate the centroid energies of the isoscalar L=0, 1 and 2 resonances with the accuracy of 0.1 MeV, comparable to the experimental uncertainties.

We have demonstrated that the spurious state mixing due to the non-zero smearing width and a choice of a coarse sized radial mesh can be accurately eliminated using the projection operator  $f_{\eta}$ . Furthermore, we show that the SSM due to a small value of  $E_{ph}^{max}$  used in the DRPA calculation can be fully eliminated by applying the projection method.

We have investigated the consequences of violation of self-consistency on the S(E)and  $\rho_t$  of the isoscalar L=0.1 and 2 giant resonances by varying the parameter  $t_0$  by  $\pm 5\%$  and  $\pm 10\%$  in the patrticle-hole interaction. We find that if the self-consistency is not maintained then the values of  $E_{ss}$  and centroid energies for the L=0, 1 and 2 isoscalar resonances are significantly different compared with their self-consistent values. Even if the particle-hole interaction is renormalized to shift  $E_{ss}$  close to its self-consistent value, the centroid energies for L=0 and 1 resonances could not be corrected. This is due to the fact that though the renormalization corrects the value of  $E_{ss}$ , the nuclear matter incompressibility coefficient,  $K'_{nm}$  associated with the particle-hole interaction is quite different than the one with the mean-field. However, the L=2 resonance is not very sensitive to the self-consistency violation as long as the particle-hole interaction is renormalized to shift  $E_{ss}$  close to its self-consistent value. It is also important to point out that the violation of self-consistency causes a significant redistribution of the transition strength. In particular, energy weighted transition strength of the lower energy component (E < 20 MeV) of the ISGDR response function may differ by 50%. The values of the SSM probabilities  $b_n^2$  were found to be less than 1-2%. Therefore, one can neglect the renormalization of the ISGDR strength function obtained using projection operator  $f_{\eta}$ . Further, we found that the total energy weighted transition strength for the operator  $f_{\eta}$  remains unaltered even with the violation of self-consistency.

Calculations were also carried out by changing the parameters appearing in the particle-hole interaction in such a way that the nuclear matter incompressibility coefficient associated with it remains unaltered. We find that though the incompressibility coefficient associated with the particle-hole and the mean field are kept the same, due to the lack of self-consistency, the centroid energy for L = 0 and 1 isoscalar resonances are off by 10% and 3.5%, respectively, compared to their self-consistent values. We may remark that if the ISGMR centroid energy is determined with accuracy of 10%, the value of  $K_{nm}$  deduced from a comparison with experimental data is then accurate

within only 20%.

This work was supported in part by the US Department of Energy under grant no. DOE-FG03-93ER40773.

# REFERENCES

- A. Bohr and B. Mottelson, Nuclear Structure (W. A. Benjamin, London, 1975),
   Vol. II, Chap. 6.
- [2] S. Stringari, Phys. Lett. **108B**, 232 (1982).
- [3] S. Shlomo and D. H. Youngblood, Phys. Rev. C 47, 529 (1993), and references therein.
- [4] J. P. Blaizot, Phys. Rep. **64**, 171 (1980).
- [5] H. L. Clark, Y.-W. Lui and D. H. Youngblood, Phys. Rev. C63 (2001) 03130, and references therein.
- [6] I. Hamamoto, H. Sagawa, and X. Z. Zhang, Phys. Rev. C 57, R1064 (1998).
- [7] A. Kolomiets, O. Pochivalov, and S. Shlomo, Progress in Research, Cyclotron Institute, Texas A&M University, April 1, 1998 March 31, 1999, III-1 (1999).
- [8] M. L. Gorelik, S. Shlomo and M. H. Urin, Phys. Rev. C 62, 044301 (2000).
- [9] S. Shlomo and A. I. Sanzhur, Phys. Rev. C 65, 044310 (2002); S. Shlomo, Pramana-J. 57, 557 (2001).
- [10] G. Colo, N. Van Giai, P. F. Bortignon and M. R. Quaglia Phys. Lett. B485, 362 (2000).
- [11] D. Vretenar, A. Wandelt, and P. Ring Phys. Lett. **B487**, 334 (2000).
- [12] J. Piekarewicz, Phys. Rev. C 62, 051304 (2000).
- [13] T. S. Dumitrescu, and F. E. Serr, Phys. Rev. C 27, 811 (1983).
- [14] H. P. Morsch, M. Rogge, P. Turek, and C. Mayer-Boricke, Phys. Rev. Lett. 45, 337 (1980).
- [15] C. Djalali, N. Marty, M. Morlet, and A. Willis, Nucl. Phys. A380, 42 (1982).

- [16] B. Davis et al., Phys. Rev. Lett. 79, 609 (1997).
- [17] G. F. Bertsch and S. F. Tsai, Phys. Rep. 18, 125 (1975).
- [18] S. Shlomo and G. F. Bertsch, Nucl. Phys. A243, 507 (1975).
- [19] I. Hamamoto and H. Sagawa, nucl-th/0207063.
- [20] B. K. Agrawal and S. Shlomo, Cyclotron Institute, Texas A & M University III-19, III-21 and III-22, 2001 (unpublished).
- [21] G. F. Bertsch, Suppl. Progr. Theor. Phys. **74**, 115 (1983).
- [22] D. Vautherin and D. M. Brink, Phys. Rev. C 5, 626, (1975)
- [23] J. V. Noble, Ann. Phys. **67**, 98 (1971).
- [24] T. J. Deal and S. Fallieros, Phys. Rev. C 7, 1709 (1973).

### **FIGURES**

- FIG. 1. Comparison of fully self-consistent HF-CRPA result for spurious state transition density (in arbitrary units) obtained using operator  $f_1$  in Eq. (6) with the corresponding coherent state transition density. The HF-CRPA calculation is carried using radial mesh size dr = (0.04, 0.04) with no smearing width ( $\Gamma = 0$  MeV).
- FIG. 2. Free response functions for ISGDR calculated using radial mesh size dr = (0.04, 0.04) with  $\Gamma/2 = 0.025$  MeV and  $\eta = 24.51$  fm<sup>2</sup>. The long dashed curve clearly manifests the existence of the spuriocity over the entire range of excitations but predominant for the  $1\hbar\omega$  region (E < 20 MeV).
- FIG. 3. Same as Fig. 2 but for fully self-consistent HF-CRPA results. The response for the operator  $f_3$  and  $f_{\eta}$  is almost the same due to no spurious state mixing.
- FIG. 4. Free and self-consistent HF-CRPA results for the ISGMR strength function calculated using radial mesh dr = (0.04, 0.04),  $\Gamma/2 = 0.025$  MeV.

## FIG. 5. Same as Fig. 4 but for ISGQR.

- FIG. 6. Strength functions for the spurious state and ISGDR calculated using radial mesh size of 0.04 fm and smearing parameter  $\Gamma/2 = 1$  MeV in CRPA. The SSM caused due to long tail of spurisous state is projected out using the operator  $f_{\eta}$ .
- FIG. 7. Discretised RPA results for ISGDR response obtained using different values of the smearing parameter (a)  $\Gamma/2 = 0.25$  MeV and (b)  $\Gamma/2 = 1.0$  MeV. The discretization is performed using  $N_{HF} = 150$  (dotted line) and  $N_{HF} = 900$  (solid line) with dr = (0.08, 0.24). We use particle-hole cut-off energy  $E_{ph}^{max} = 200$  MeV.

- FIG. 8. Comparison of the spurious state transition density obtained using discretized RPA and collective model (dotted line). The dash-dot, long dash and solid curves represent the DRPA results for  $N_{HF}$  ( $E_{ph}^{max}$ ) = 150 (50 MeV), 900 (50 MeV), 900 (200 MeV), respectively. The values of transition density do not change significantly when  $N_{HF}$  increased from 150 to 900, but, with increase in  $E_{ph}^{max}$  the DRPA results become closer to the collective model results.
- FIG. 9. The centroid energies  $E_0$  and  $E_1$  versus  $\sqrt{K'_{nm}}$  for  $^{80}Zr$ . Here,  $K'_{nm}$  denotes the nuclear matter incompressibility coefficient associated with the parameters used in particle-hole interaction (see also the text).
- FIG. 10. Non self-consistent CRPA results for the ISGDR strength functions for the operators  $f_3$  and  $f_{\eta}$  calculated using  $t_0 = -1620 \text{ MeVfm}^3$ , radial mesh size dr = (0.04, 0.04) and  $\Gamma/2 = 0.25 \text{ MeV}$ . The strength function for the operator  $f_{\eta}$  is larger than that for the operator  $f_3$  for a wide range of energy.
- FIG. 11. Influence of violation of self-consistency due to variation of  $t_0$  by +5% (dashed line) and -5% (dotted line) on the strength function for (a) ISGMR, (b) ISGDR and (c) ISGQR. Solid line represents the self-consistent result (i.e.,  $t_0$ =-1800 MeVfm<sup>3</sup>).
- FIG. 12. Comparison of DRPA results for ISGDR strength functions obtained for (a)  $t_0 = -1800$ , (b)  $t_0 = -1620$  and (c)  $t_0 = -1980$  MeV fm<sup>3</sup>. Numerical calculations for all the cases are performed using,  $N_{HF} = 150$ , dr = (0.08, 0.24),  $E_{ph}^{max} = 50$  and  $\Gamma/2 = 0.25$  MeV.

FIG. 13. Same as Fig. 12 but for  $E_{ph}^{max}=200$  MeV.

TABLES

TABLE I. Hartree-Fock single particle energies (in MeV) for the bound states in  $^{80}Zr$  nucleus obtained with the interaction parameters  $t_0=-1800$  MeVfm<sup>3</sup>,  $t_3=-12871$  MeVfm<sup>4</sup> and  $\alpha=1/3$  using the small mesh size dr=0.04 fm.

Orbits	0s	0p	0d	1s	0f	1p	0g	1d	2s
Energy	-45.50	-39.14	-31.02	-26.74	-21.42	-15.33	-10.59	-3.98	-2.62

TABLE II. Values for density radial moments  $\langle r^2 \rangle$  and  $\langle r^4 \rangle$  in units of fm<sup>2</sup> and fm<sup>4</sup>, respectively, together with the EWSR associated with the scattering operator  $r^n Y_{LM}$ , in units of fm<sup>(2n)</sup>MeV, for different mesh size dr (in fm) used in the HF calculations.

				EWSR					
dr	$\langle r^2 \rangle$	$\langle r^4 \rangle$	$rY_{10}$	$r^3Y_{10}$	$(r^3 - \eta r)Y_{10}$	$r^2Y_{00}$	$r^2Y_{20}$		
0.04	14.705	282.147	391.04	404545	169661	7667	19167		
0.08	14.702	282.008	391.04	404346	169553	7665	19163		
0.24	14.676	280.653	391.04	402403	168441	7651	19129		

TABLE III. The energy weighted transition strengths  $(S^{EW})$  of the free and fully self-consistent HF-CRPA for  $^{80}Zr$  nucleus (in fm<sup>6</sup>MeV) calculated using  $dr_{HF} = dr_{RPA} = 0.04$  fm,  $N_{RPA} = 300$  with no smearing width ( $\Gamma = 0$  MeV).

Free response								
Energy	$S_3^{EW}$	$-2\eta S_{13}^{EW}$	$\eta^2 S_1^{EW}$	$S^{EW}_{\eta}$				
10.832306	87689	-221289	139609	6009				
11.352610	47160	-99851	52854	163				
12.709777	24341	-37010	14068	1399				
17.437181	48562	-64831	21638	5369				
35.163326	17114	-7514	825	10425				
36.520494	5034	-2123	224	3135				
15.0-18.0	465	393	528	1386				
18.0-100.0	172707	-36767	5009	140949				
100.0-150.0	1256	-609	89	736				
Total	404328	-469601	234844	169571				
		CRPA response	е					
0.078606	234852	-469709	234857	0				
11.434169	4480	5	-1	4484				
12.965783	1984	7	0	1991				
15.0-18.0	6087	45	0	6132				
18.0-100.0	156848	-42	2	156808				
100.0-150.0	258	-13	1	246				
Total	404509	-469707	234859	169661				

TABLE IV. Fully self-consistent HF–CRPA results for the energy weighted transition strengths (in fm<sup>6</sup>MeV) for  $\Gamma=0$  MeV using different mesh sizes (in fm) and  $N_{RPA}=50$ .

	$dr_{RPA} = dr_{HF} = 0.24$							
Energy	$S_3^{EW}$	$-2\eta S_{13}^{EW}$	$\eta^2 S_1^{EW}$	$S_{\eta}^{EW}$				
0.714539	232751	-465617	232866	0				
11.483532	4214	-18	0	4196				
13.138693	2306	-124	2	2184				
15.0-18.0	5693	263	3	5959				
18.0-100	154096	792	11	154899				
100-150	184	-7	1	178				
Total	399244	-464711	232883	167416				
		$dr_{RPA} = 6dr_{HF} =$	0.24					
11.429694	4470	43	0	4513				
12.962171	1998	-2	-4	1992				
15.0-18.0	6158	-43	1	6116				
18.0-100.0	159022	-2693	45	156374				
100.0-150.0	363	-126	19	256				
Total	172011	-2821	61	169251				
	$dr_{RP}$	$A_A = 6dr_{HF} = 0.24, V_S$	$s_{c} = 0.9916^{a}$					
0.099965	237622	-474392	236771	1				
11.430431	4505	-27	0	4478				
12.959961	2025	-20	0	2005				
15.0-18.0	6288	-157	3	6134				
18.0-100.0	159324	-2992	52	156384				
100.0-150.0	368	-128	19	259				
Total	410132	-477716	236845	169260				

a) Normalization of the particle-hole interaction to put the spurious state at 0.1 MeV.

TABLE V. HF based CRPA results for the spurious state energy  $E_{ss}$  and centroid energy  $E_L$  for the ISGMR (L=0), ISGDR (L=1) and ISGQR (L=2) (in MeV) obtained using  $\Gamma/2=0.025$  MeV. For L=0 and 2 resonances we use the energy range 0-80 MeV and for L=1 we use 28-80 MeV.

$dr_{hf}$	$dr_{rpa}$	$V_{sc}$	$E_{ss}$	$E_0$	$E_1$	$E_2$
0.04	0.04	1.0	0.08	22.98	35.88	14.67
0.08	0.08	1.0	0.18	22.97	35.86	14.70
0.24	0.24	1.0	0.71	22.92	35.80	14.69
0.04	0.24	1.0	*)	22.94	35.83	14.60
0.04	0.24	0.9916	0.09	22.98	35.85	14.70
0.04	0.24	0.9707	2.00	23.08	35.88	14.96

 $<sup>\</sup>overline{*}^{}E_{ss}$  is imaginary.

TABLE VI. HF-CRPA results for fraction energy weighted sum rule (in percent) for the spurious state (SS) and for L=0-2 resonances calculated using various radial mesh sizes  $dr_{HF}$  and  $dr_{RPA}$  (in fm) and the energy region 0 - 80 MeV for  $\Gamma/2=0.025$  MeV\*. See Table V for the corresponding values of  $E_{ss}$ .

$dr_{HF}$	$dr_{RPA}$	$V_{scale}$	SS	L = 0	L=1	L=2
0.04	0.04	1.0	99.99	99.84	99.61	99.91
0.08	0.08	1.0	99.95	99.76	99.76	99.91
0.24	0.24	1.0	99.55	99.74	99.25	99.49
0.04	0.24	1.0		102.05	99.57	101.18
0.04	0.24	0.9916	101.22	102.02	99.57	101.17
0.04	0.24	0.9707	101.58	102.96	99.34	101.15

<sup>\*</sup>For the spurious state we use  $\Gamma = 0$  and Eq.(8).

TABLE VII. CRPA results for the fraction energy weighted sum rule (in percent) of the ISGDR obtained using the operator  $f_{\eta}$  for the energy range  $\omega_1 - \omega_2$  (in MeV) for various combinations of the mesh size (in fm) and smearing parameter  $\Gamma/2$  (in MeV).

				$\omega_1 - \omega_2$			
$dr_{HF}$	$dr_{RPA}$	$\Gamma/2$	0 - 15	15 - 18	18 - 100	100 - 150	Total
0.04	0.04	0.0	3.82	3.61	92.42	0.15	100.00
0.04	0.04	0.025	3.81	3.59	92.40	0.16	99.96
0.04	0.04	0.25	3.79	3.33	92.38	0.27	99.77
0.04	0.04	1.0	3.69	2.89	91.87	0.65	99.10
0.24	0.24	0.0	3.79	3.54	91.96	0.11	99.40
0.24	0.24	0.025	3.78	3.51	91.95	0.12	99.36
0.24	0.24	0.25	3.75	3.29	91.91	0.23	99.18
0.24	0.24	1.0	3.63	2.88	91.39	0.61	98.51
0.04	0.24	0.0	3.83	3.60	92.17	0.15	99.75
0.04	0.24	0.025	3.83	3.48	92.16	0.16	99.63
0.04	0.24	0.25	3.80	3.33	92.13	0.28	99.54
0.04	0.24	1.0	3.71	2.89	91.62	0.65	98.87
0.04*	0.24	0.0	3.82	3.61	92.17	0.15	99.75
0.04*	0.24	0.025	3.82	3.49	92.17	0.16	99.64
0.04*	0.24	0.25	3.79	3.34	92.14	0.28	99.55
0.04*	0.24	1.0	3.69	2.90	91.63	0.66	98.88

 $<sup>^*</sup>V_{sc} = 0.9916$  and  $E_{ss} = 0.1$  MeV.

TABLE VIII. HF-DRPA results for  $E_{ss}$  and the fraction of energy weighted sum rule of the ISGDR obtained using  $f_{\eta}$  (in percent) in the energy range  $\omega_1 - \omega_2$  for various combinations of  $N_{HF}$ ,  $E_{ph}^{max}$  and  $\Gamma/2$  with  $V_{sc}=1.0$ ,  $N_{RPA}=50$ ,  $dr_{HF}=0.08$  fm and  $dr_{RPA}=0.24$  fm. Values of  $\omega$ ,  $E_{ss}$ ,  $E_{ph}^{max}$  and  $\Gamma/2$  are in MeV.

				$\omega_1-\omega_2$				
$N_{HF}$	$E_{ph}^{max}$	$\Gamma/2$	$E_{ss}$	0 - 15	15 - 18	18 - 100	100 - 150	Total
150	50	0.25	4.4	3.65	2.74	88.74	0.00	95.13
150	200	0.25	1.3	3.81	3.07	93.22	0.42	100.52
150	400	0.25		3.84	3.07	93.22	0.41	100.54
150	50	1.0	4.3	3.71	2.80	85.71	0.00	92.22
150	200	1.0	1.1	3.89	3.02	93.29	1.21	101.41
150	400	1.0		3.92	3.03	93.26	1.21	101.42
900	50	0.25	4.7	3.64	3.11	85.01	0.00	91.77
900	200	0.25	1.5	3.79	3.43	90.68	0.44	98.34
900	400	0.25	1.0	3.82	3.43	90.67	0.44	98.36
900	50	1.0	4.6	3.70	2.80	82.82	0.00	89.32
900	200	1.0	1.4	3.88	3.03	91.16	1.22	99.29
900	400	1.0	0.7	3.90	3.04	91.15	1.21	99.30

TABLE IX. Dependence of  $E_{ss}$  and the centroid energies  $E_L$  (L=0, 1 and 2), in MeV, on the value of  $E_{ph}^{max}$  (in MeV) used in HF-DRPA calculations. We have used the values of  $N_{HF}=900$ ,  $N_{RPA}=50$ , dr=(0.08,0.24) and  $\Gamma/2=0.25$  MeV. The corresponding HF-CRPA results are placed in the last row.

$E_{ph}^{max}$	$E_{ss}$	$E_0$	$E_1$	$E_2$
50	4.7	23.92	35.34	16.11
75	3.3	23.51	35.76	15.51
100	2.9	23.25	35.66	15.14
200	1.5	23.09	35.55	14.82
400	1.0	23.02	35.51	14.73
600	0.9	23.02	35.51	14.72
$\infty$	0.7	23.01	35.46	14.70

TABLE X. HF-CRPA results for the spurious state energy  $E_{ss}$ , incompressiblity coefficient  $K'_{nm}$  and centroid energy  $E_L$  (in MeV) for isoscalar giant resonances for L=0-2 with different values of  $t_0$ ,  $t_3$  and  $V_{sc}$  used in the particle-hole interaction. These calculations are performed using  $\Gamma/2=0.25$  MeV and  $dr_{HF}=dr_{RPA}=0.04$ fm.

$t_0$	$t_3$	$V_{sc}$	$K'_{nm}$	$E_{ss}$	$E_0$	$E_1$	$E_2$
-1800	12871	1.0	226	0.1	23.1	35.5	14.8
-1710	12871	1.0	258	6.7	26.3	37.9	17.4
-1710	12871	1.2938	321	0.1	26.0	38.2	14.7
-1620	12871	1.0	289	9.2	29.0	40.0	19.5
-1620	12871	1.7118	464	0.1	29.8	41.8	14.7
-1620	11875	1.0	226	5.9	24.9	36.7	16.8
-1620	11270	1.0	188	0.1	21.6	34.4	14.8
-1890	12871	1.0	194		18.7	32.8	11.1
-1890	12871	0.7910	163	0.1	20.8	33.7	14.8
-1980	12871	1.0	162		11.4	29.9	2.1
-1980	12871	0.6398	120	0.1	19.2	32.6	14.9
-1980	13875	1.0	226		20.8	34.2	12.1
-1980	14500	1.0	266	0.1	24.3	36.6	14.7

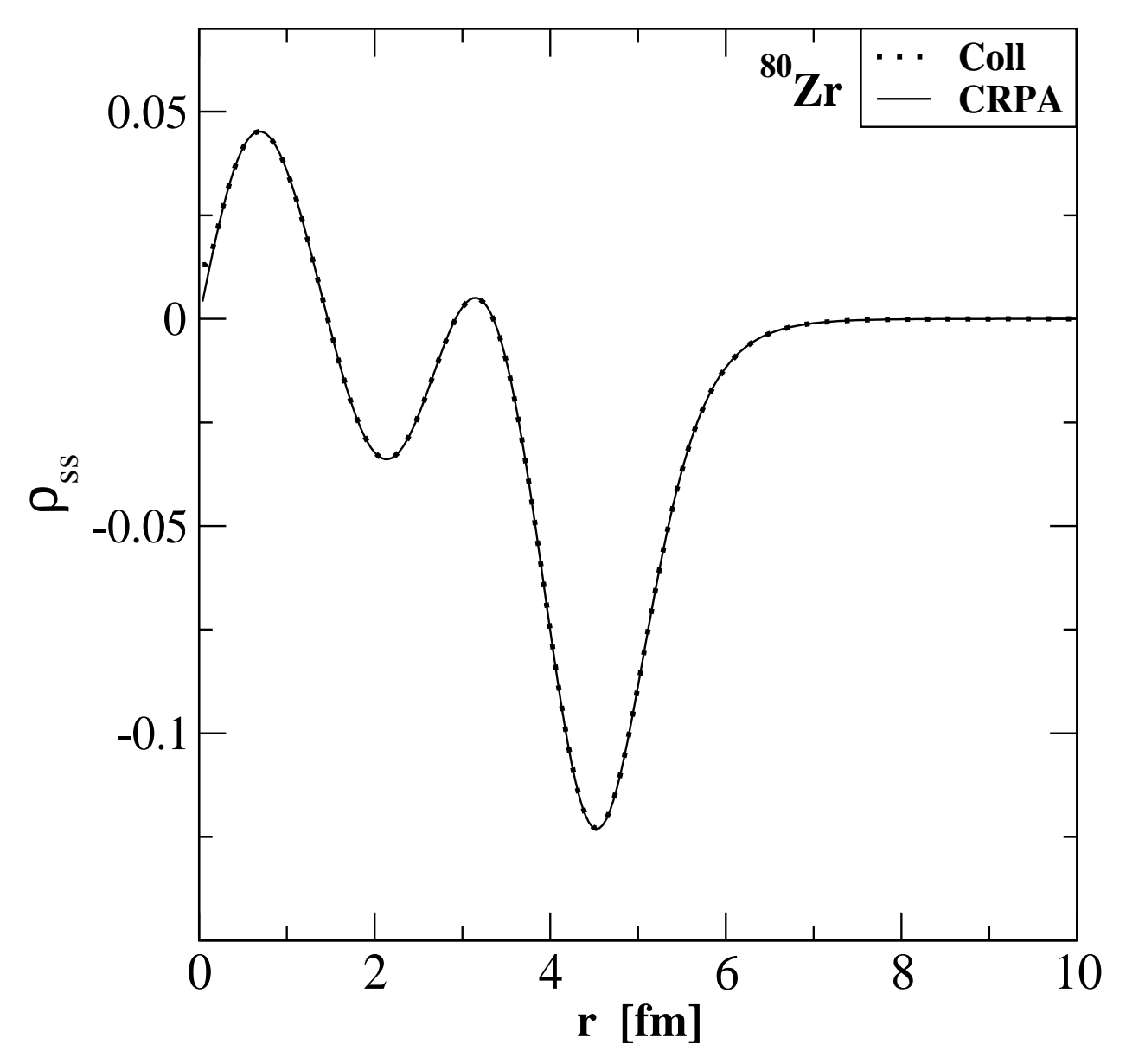


Fig. 1

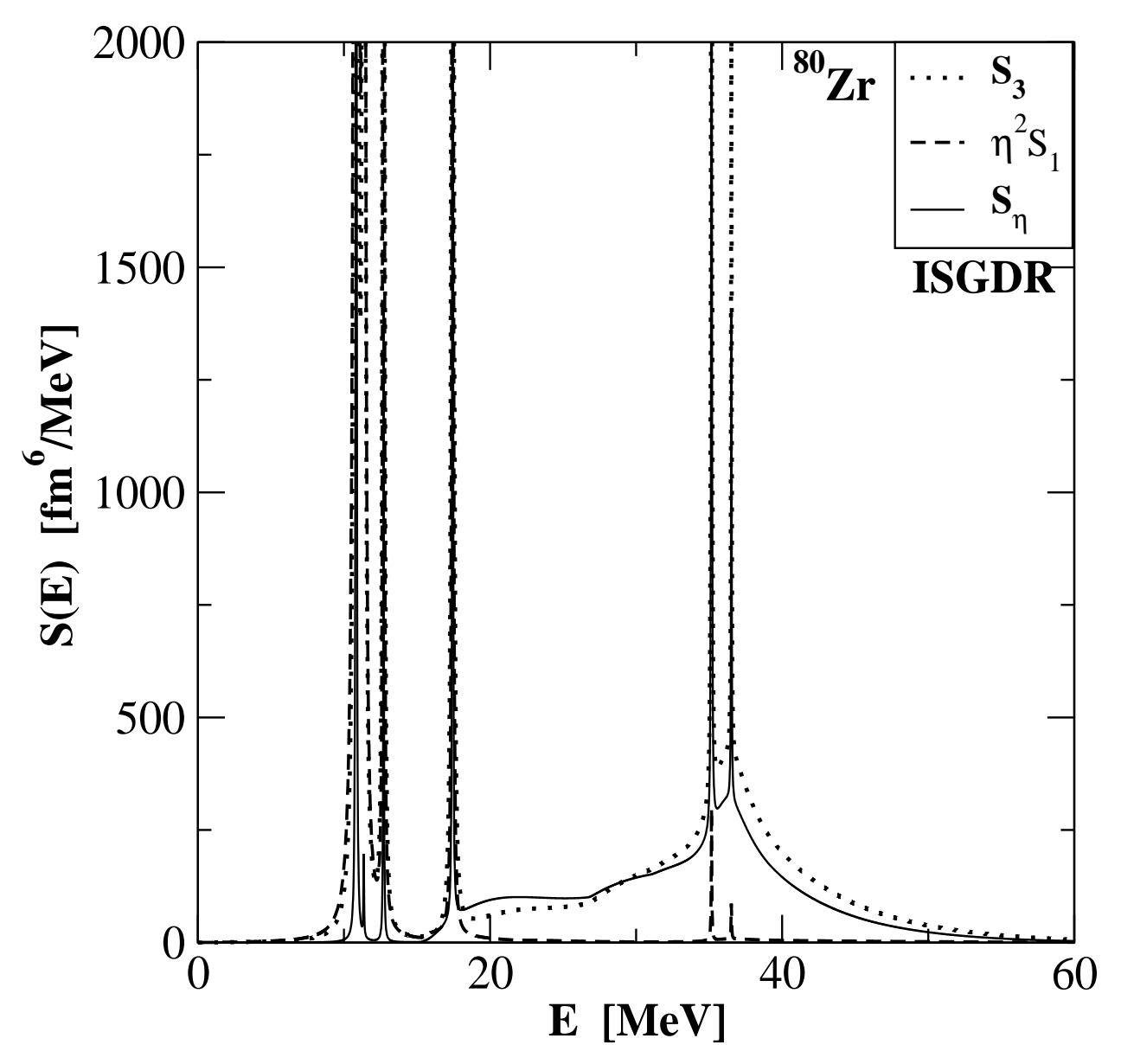


Fig. 2

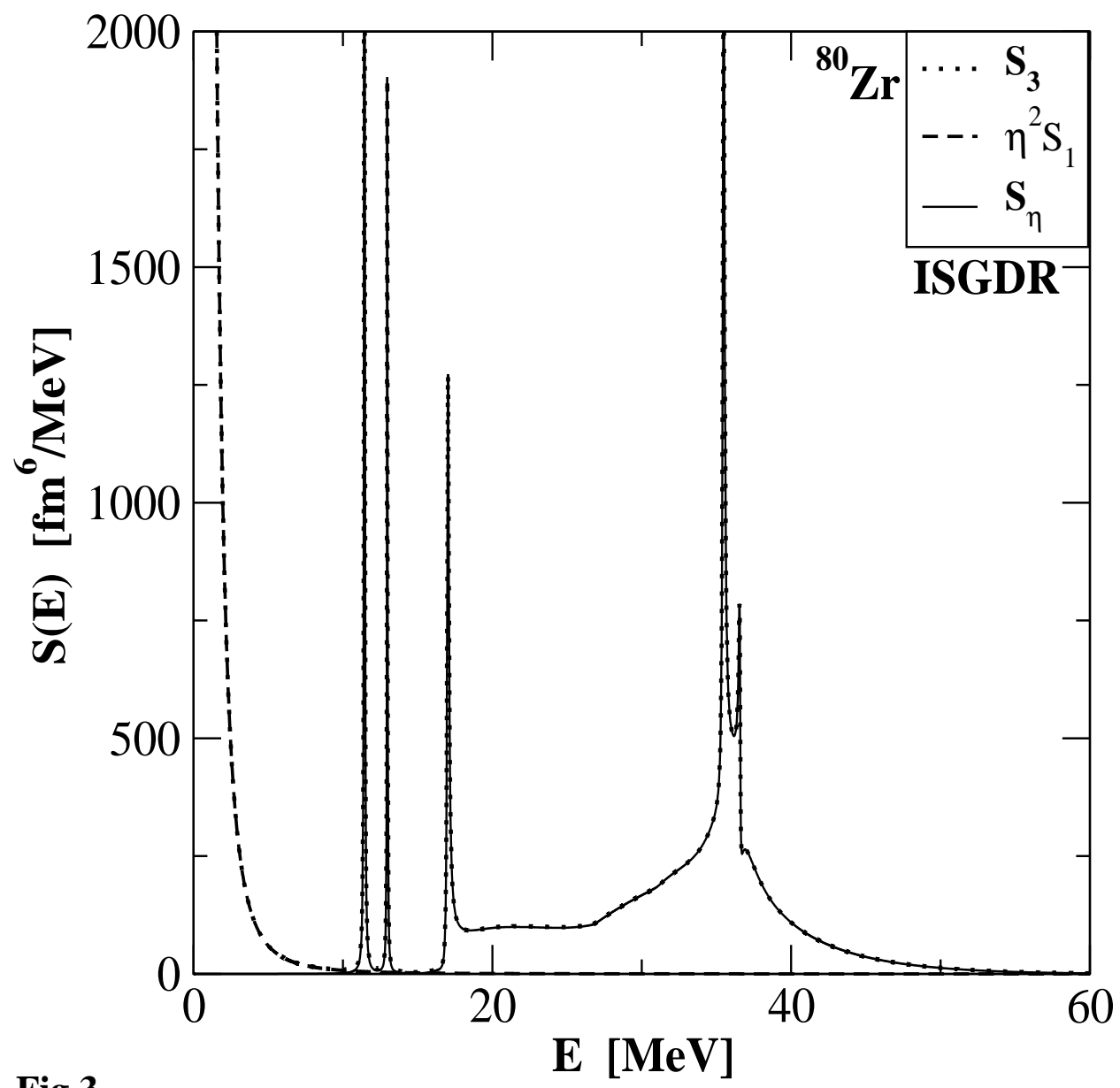


Fig.3

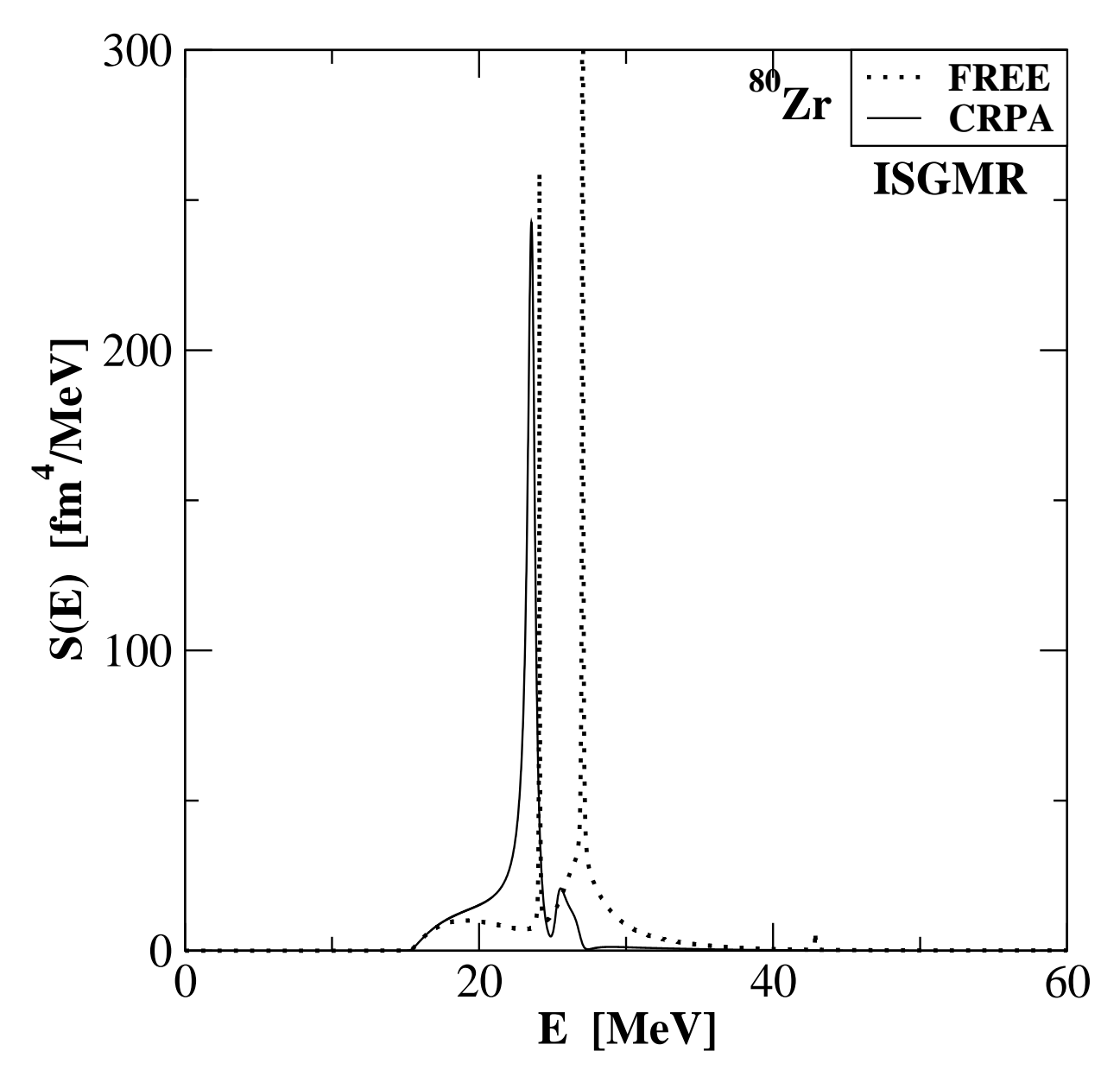


Fig. 4

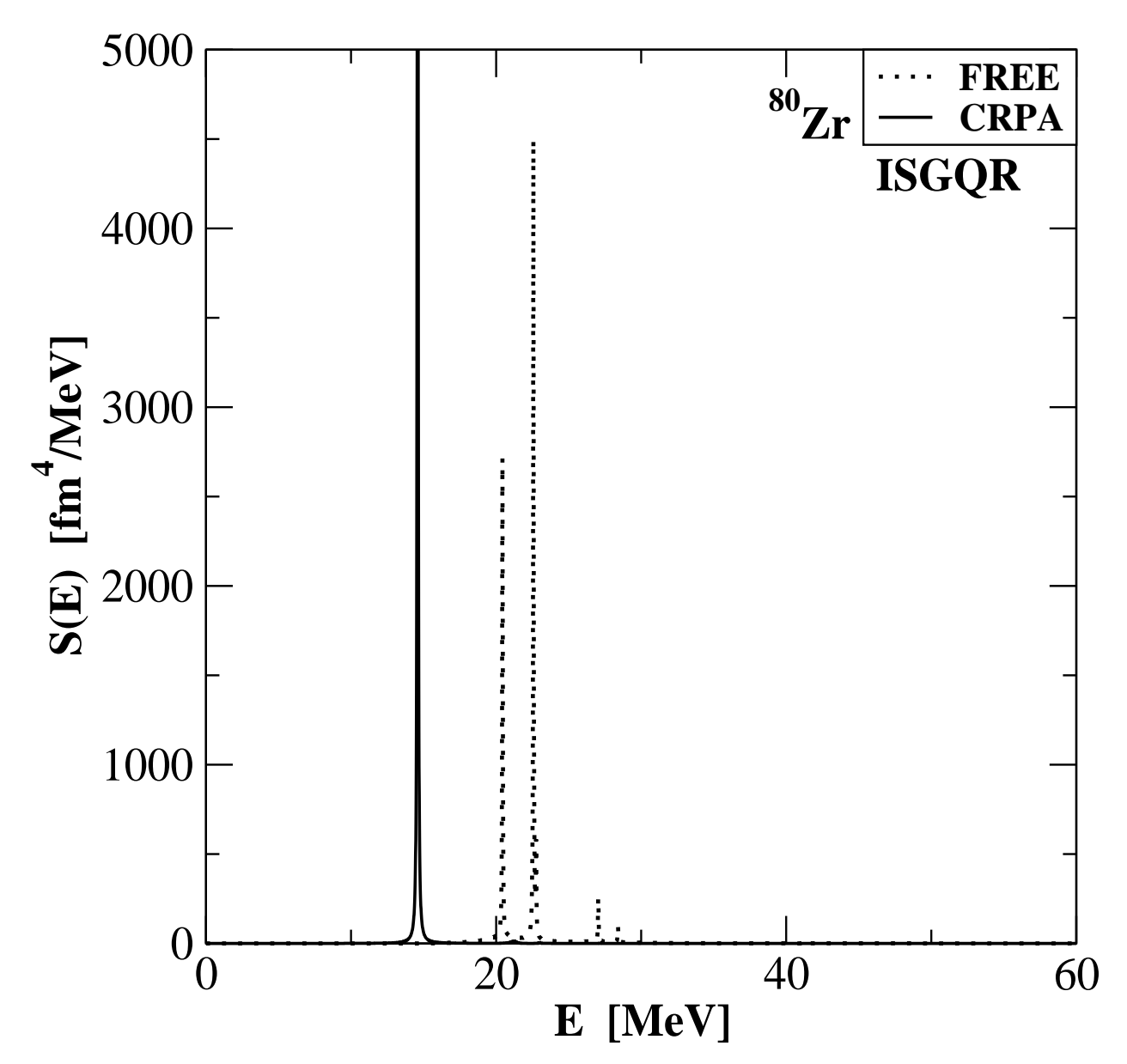


Fig. 5

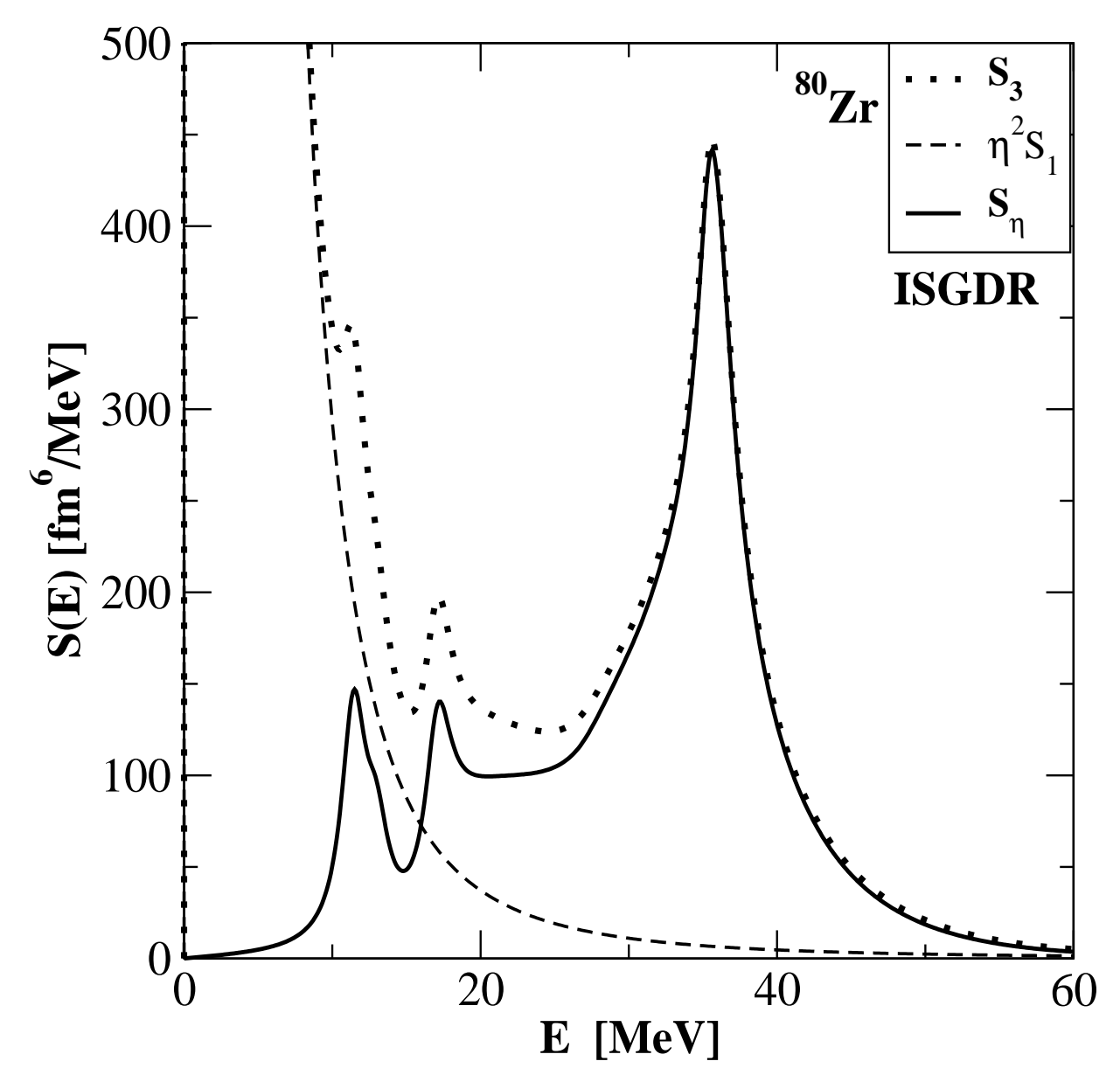


Fig.6

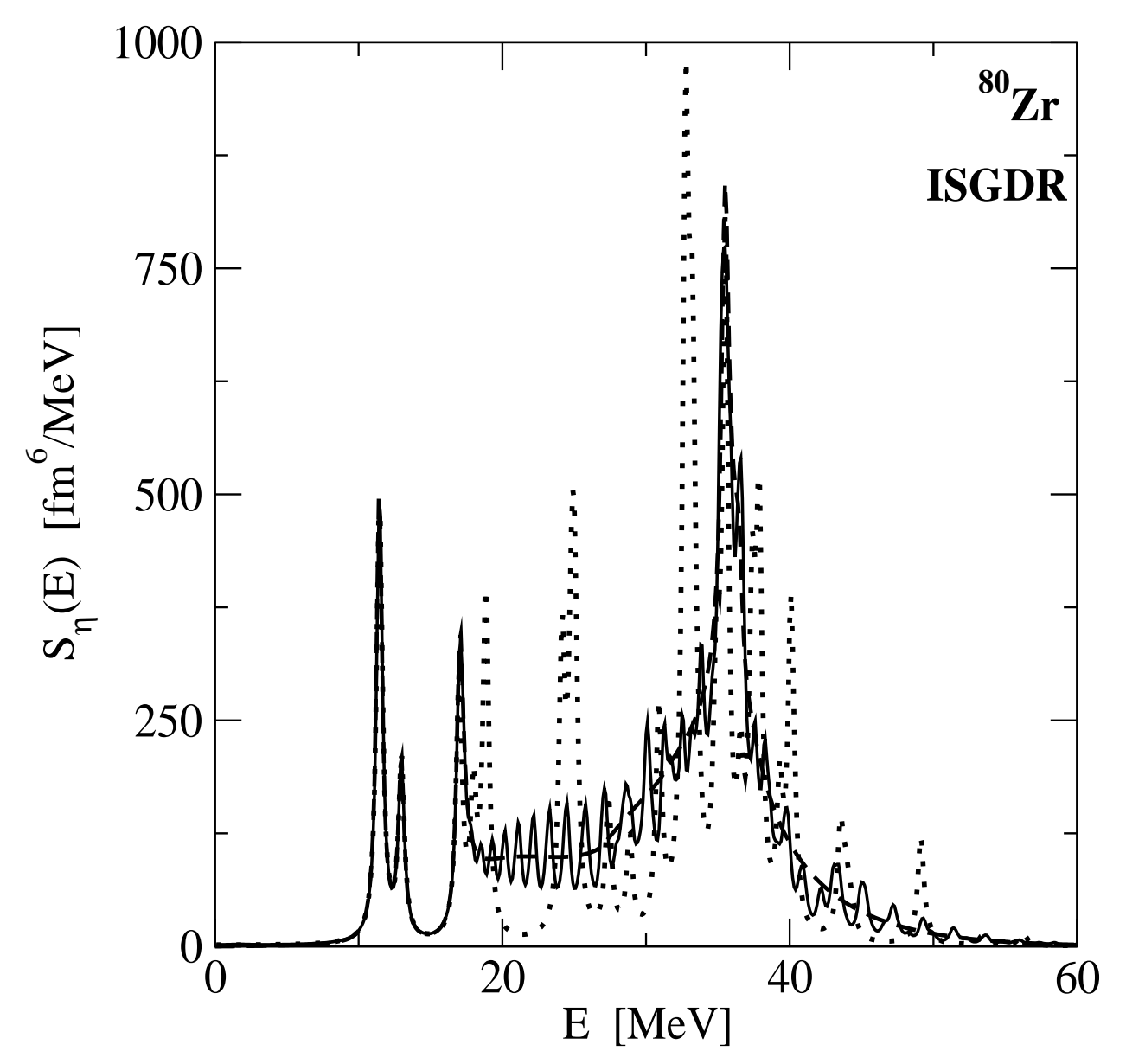


Fig. 7a

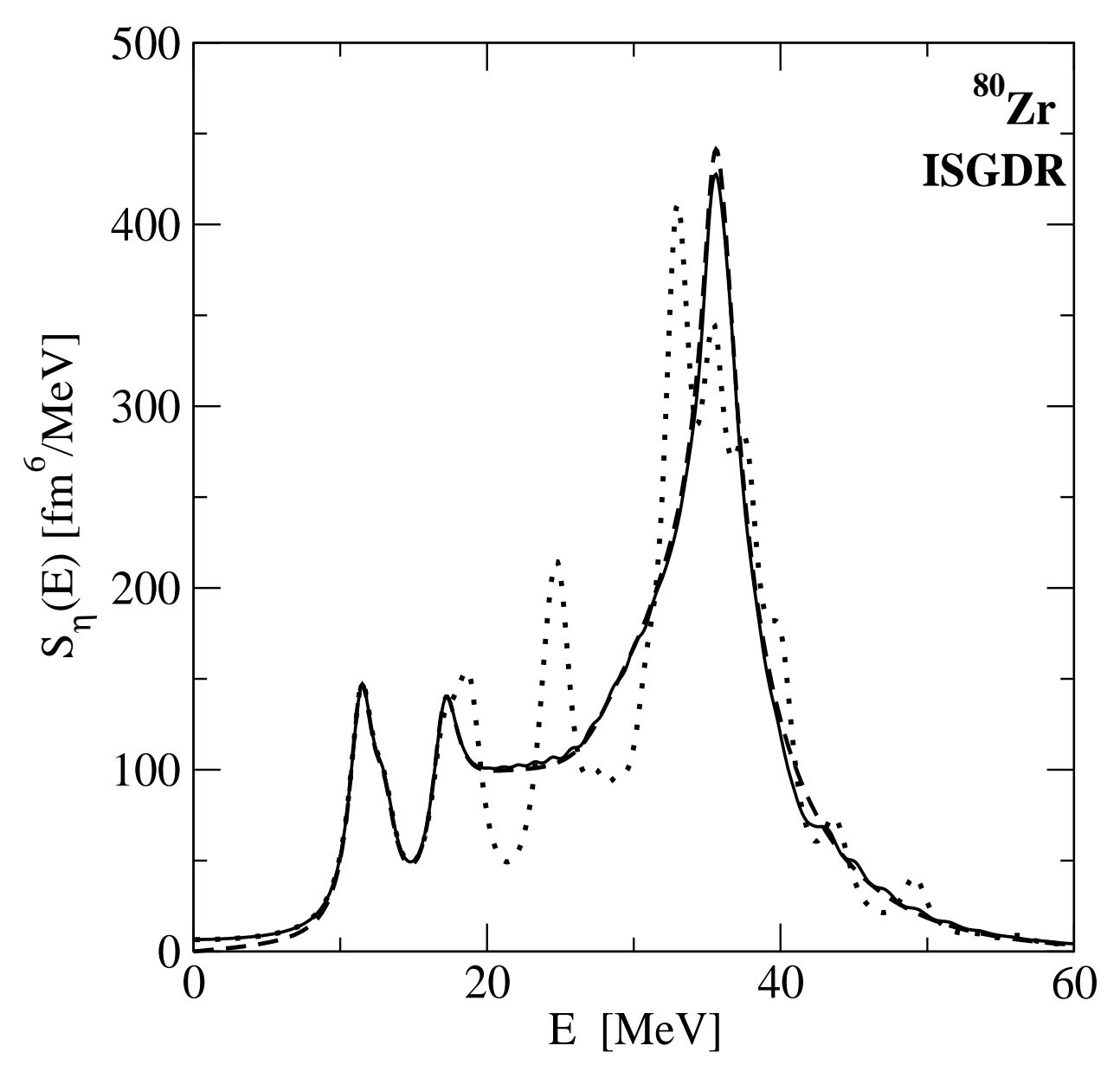


Fig. 7b

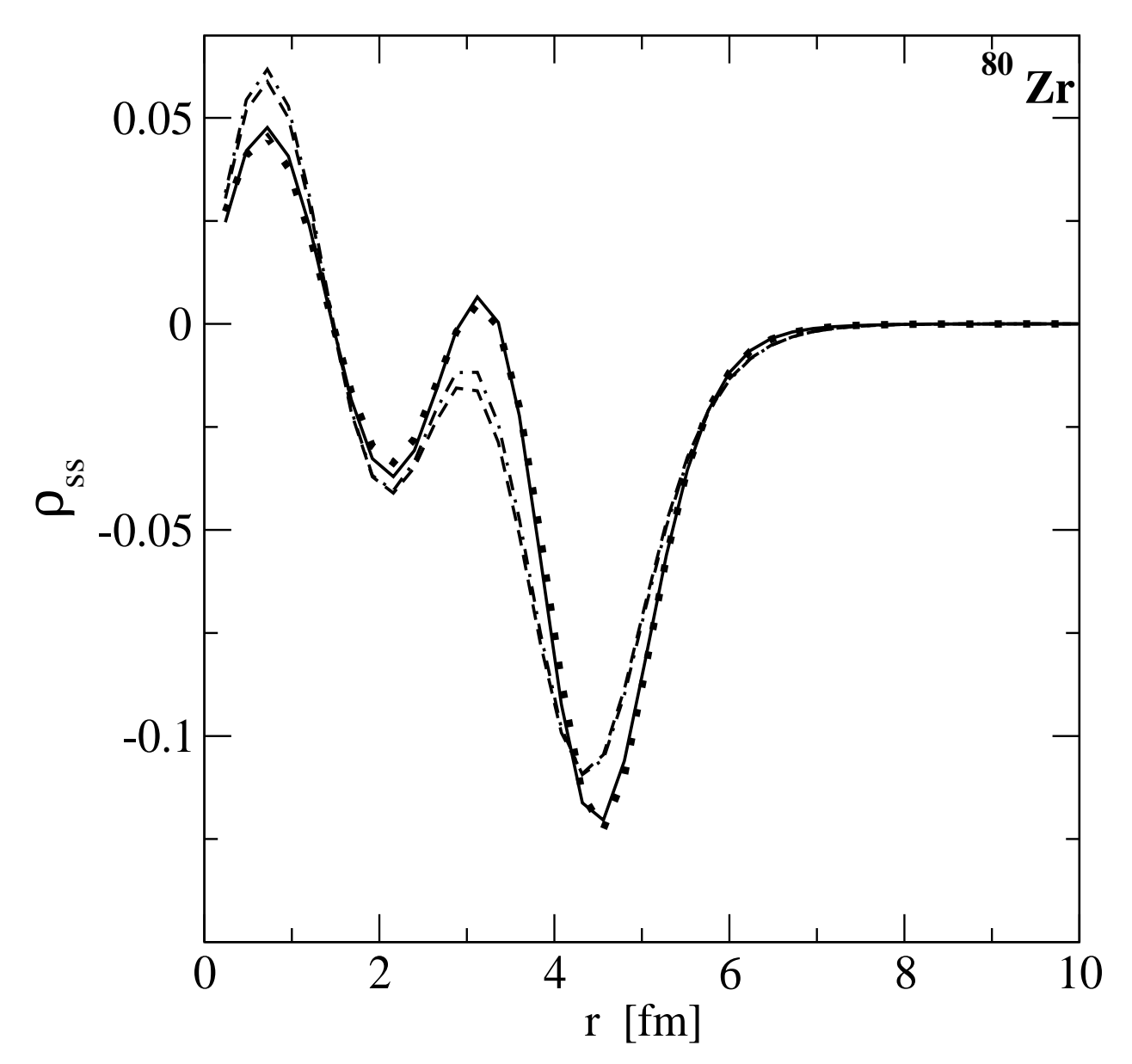


Fig. 8

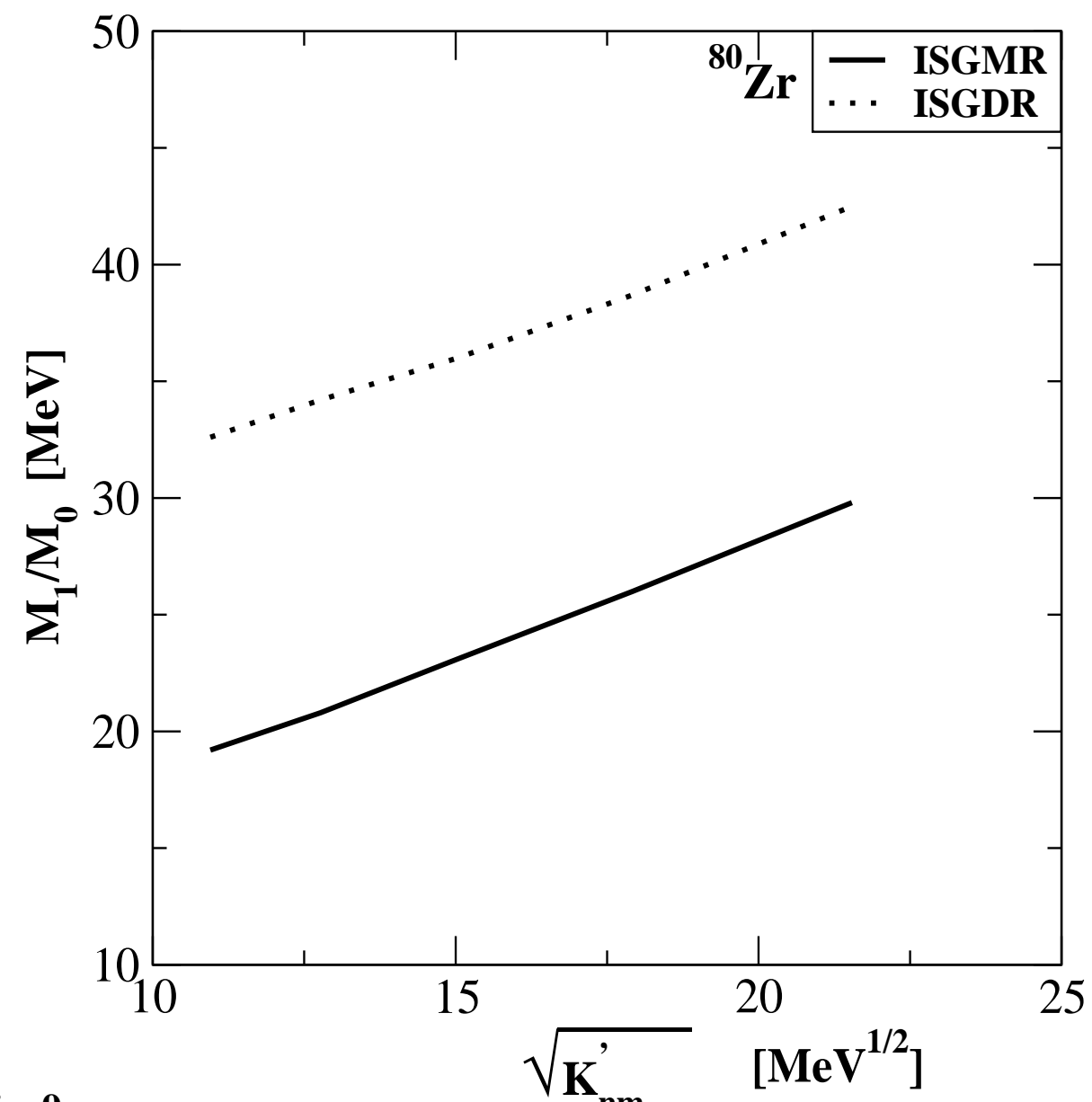
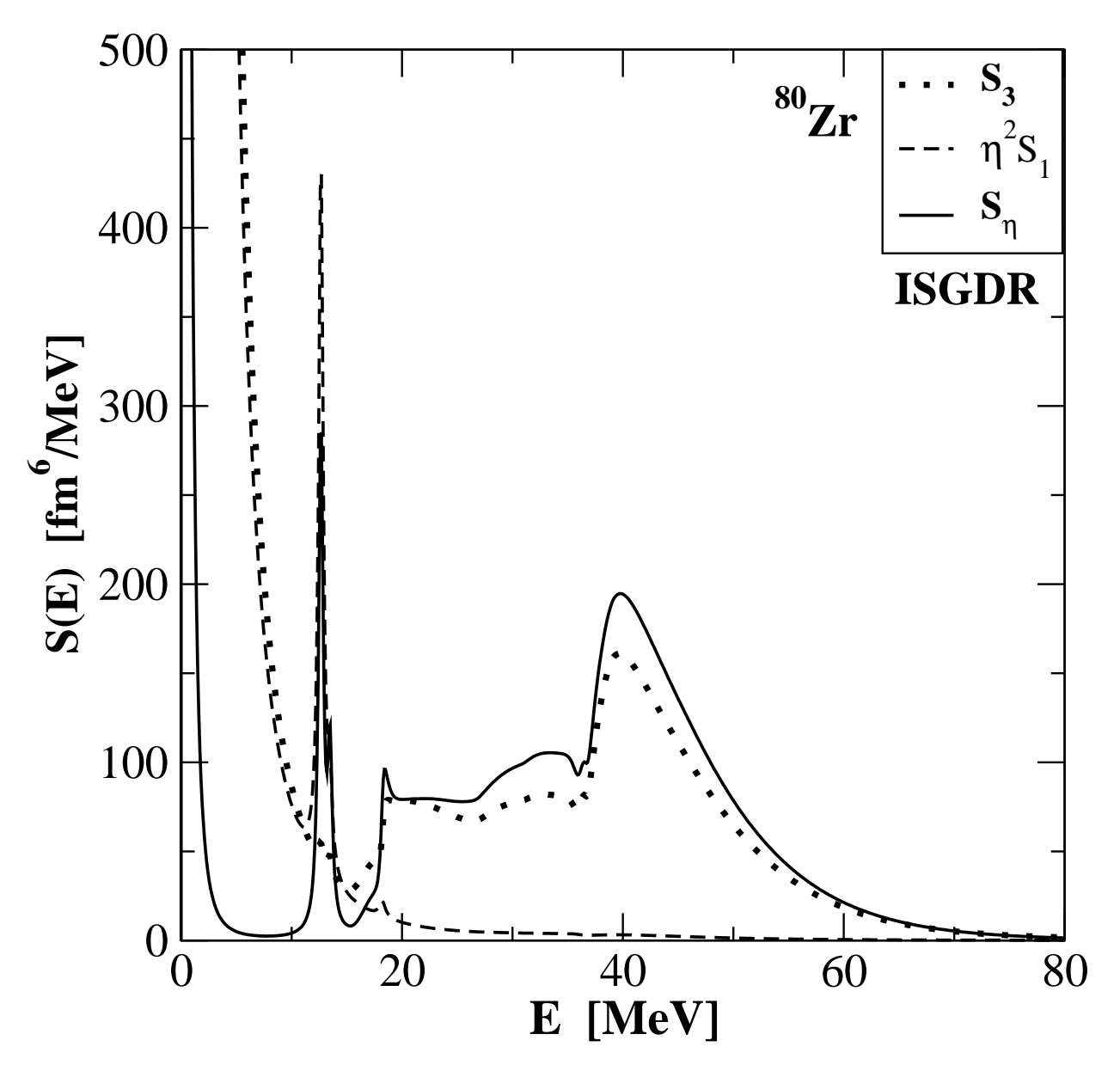
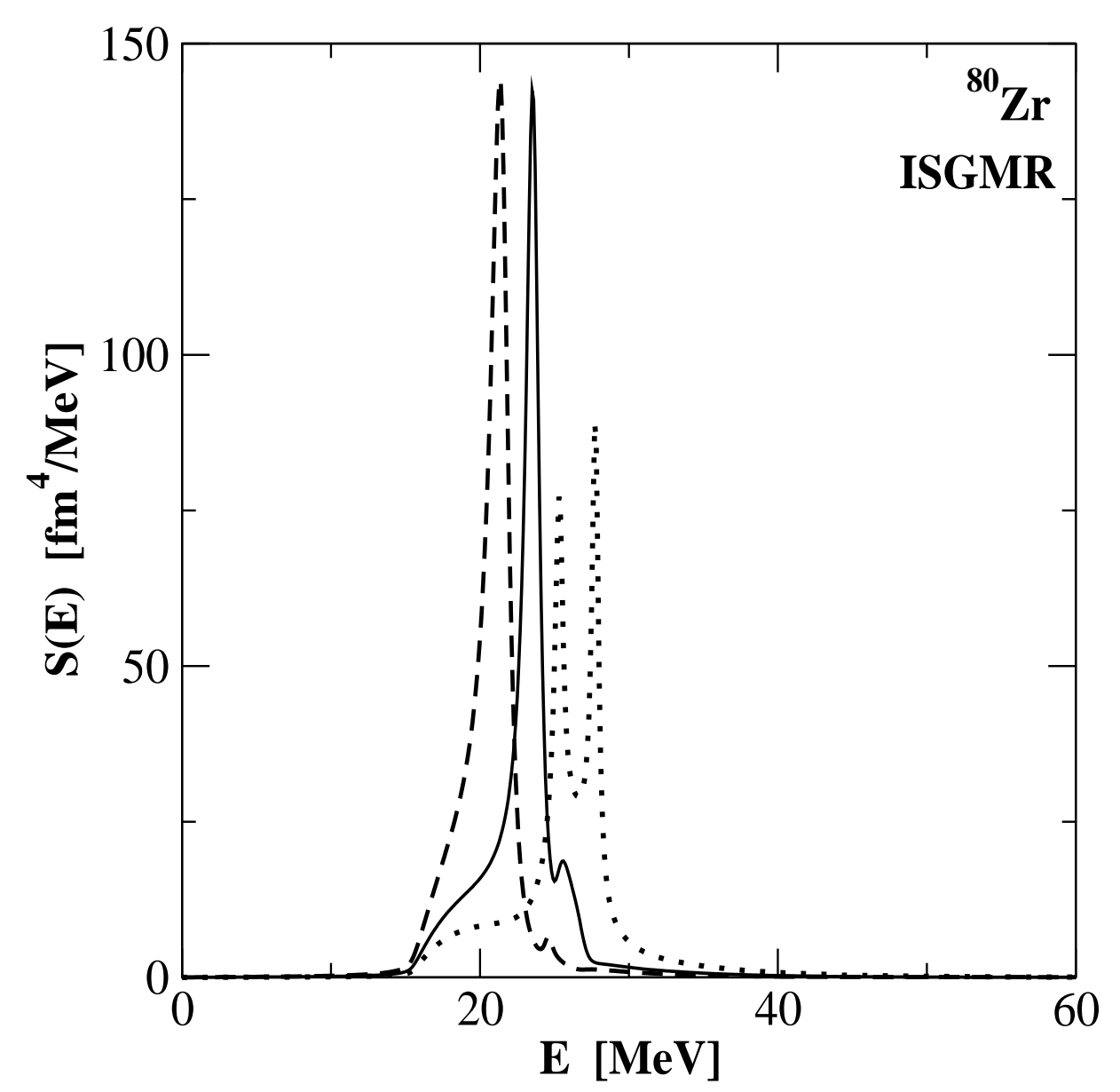


Fig. 9



**Fig. 10** 



**Fig. 11a** 

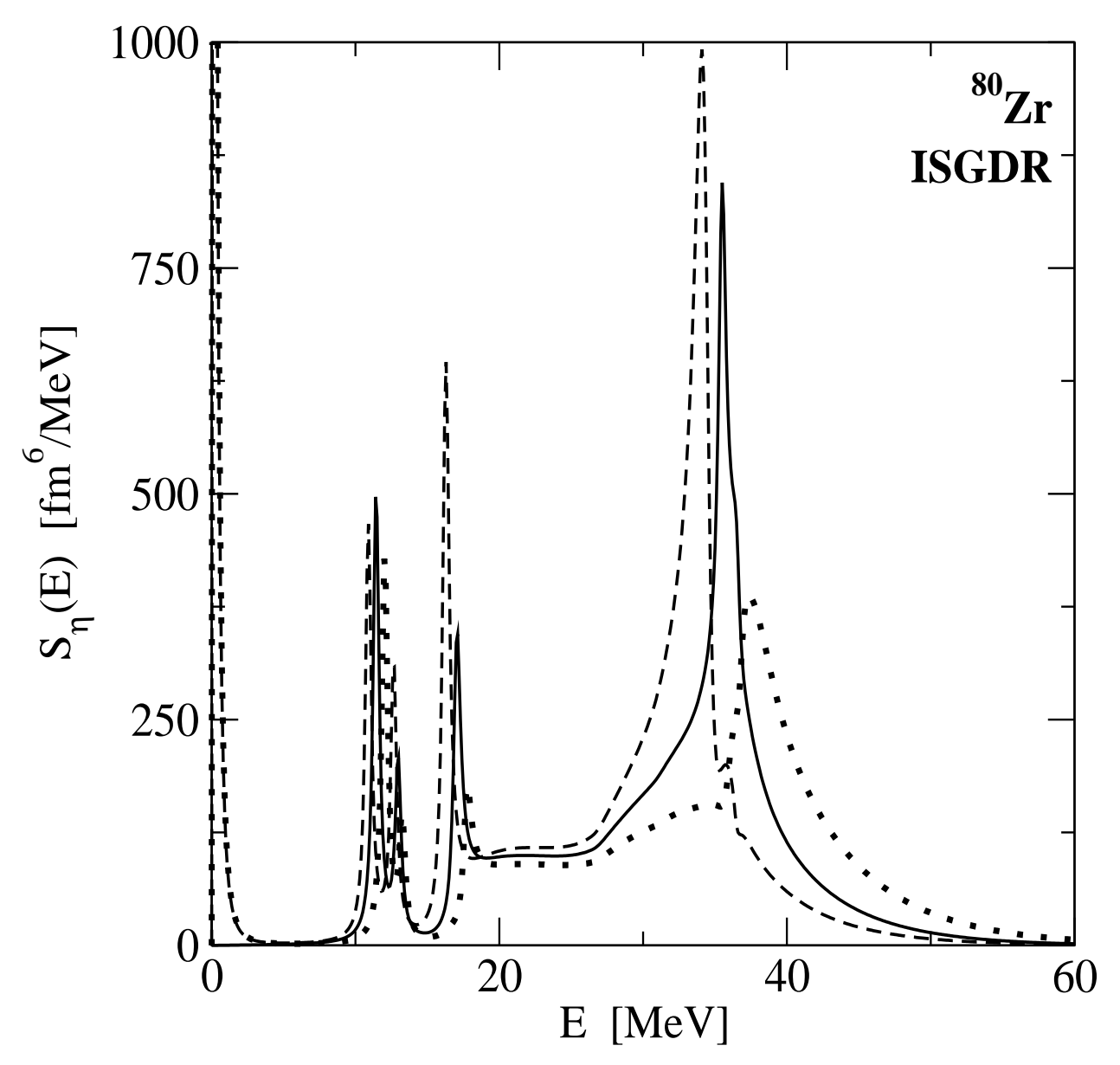


Fig. 11b

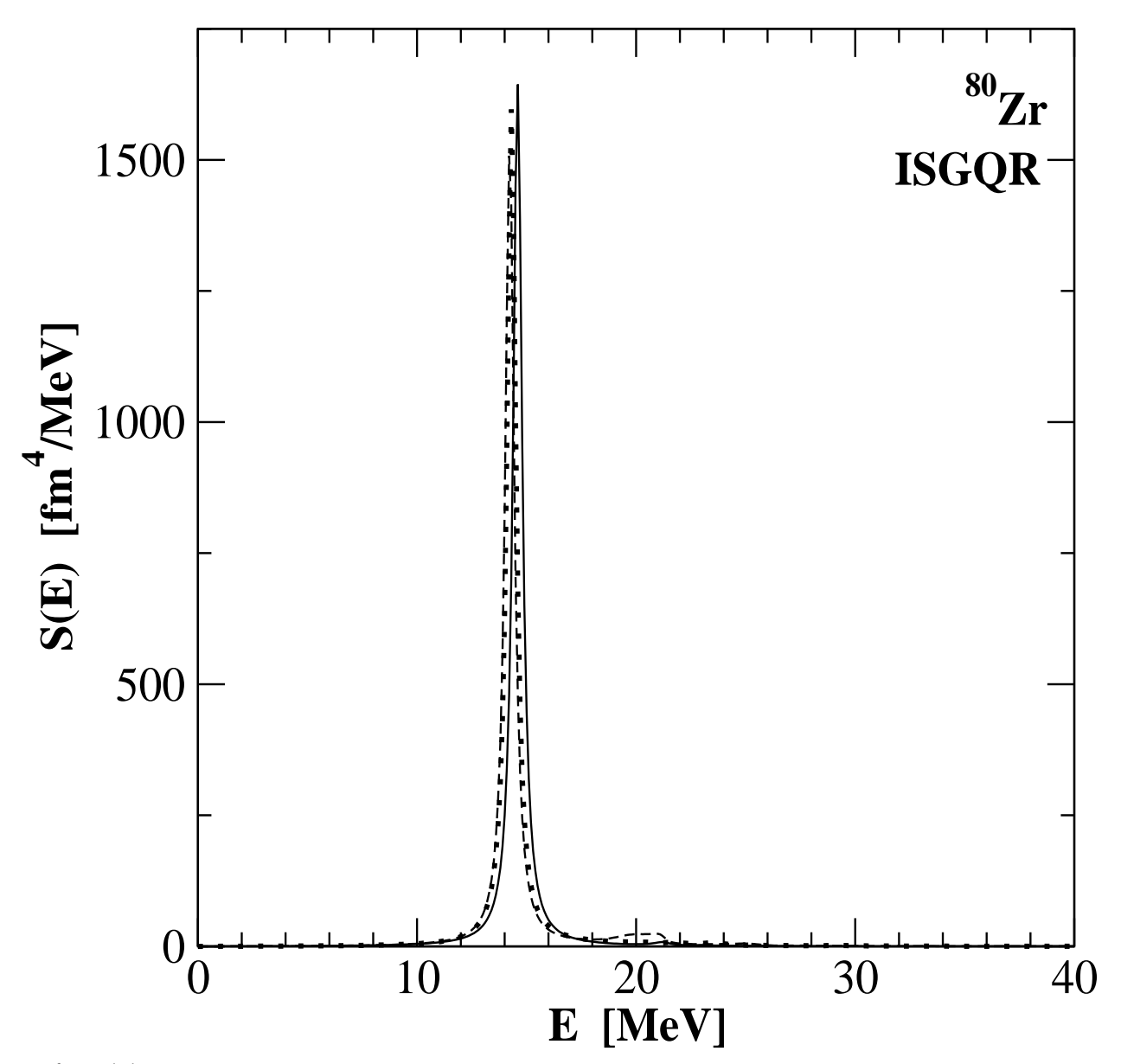
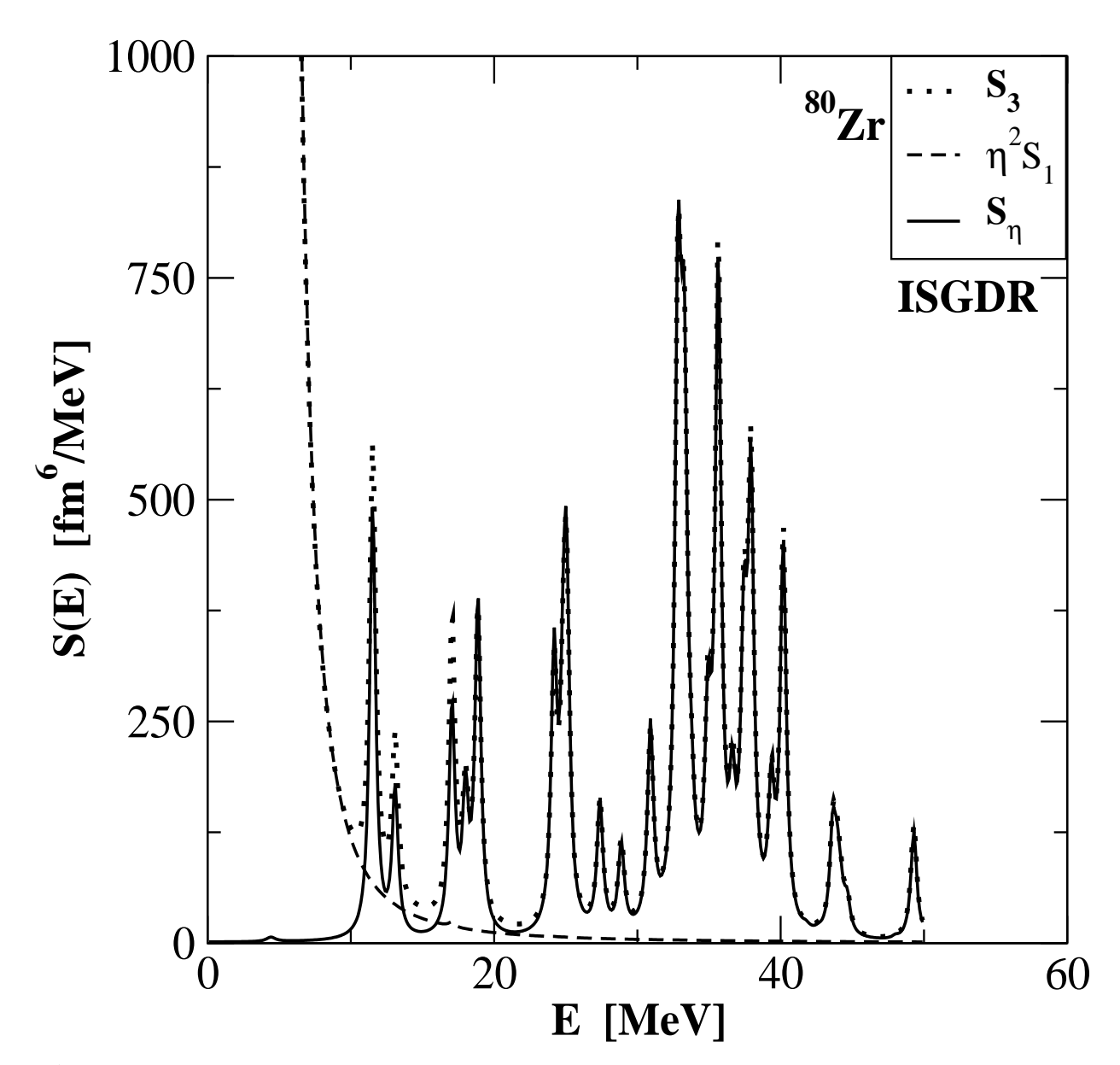


Fig. 11c



**Fig. 12a** 

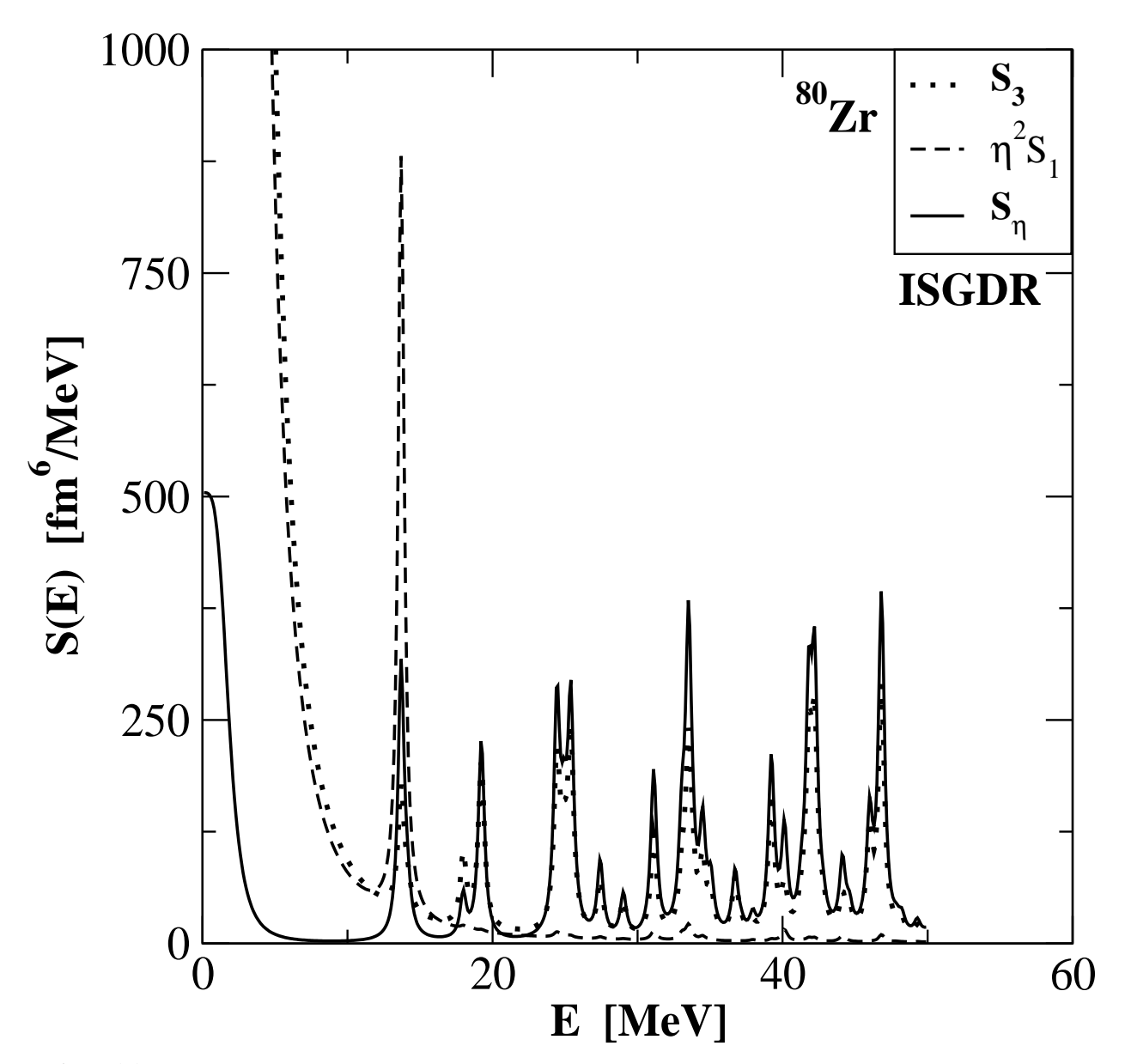


Fig. 12b

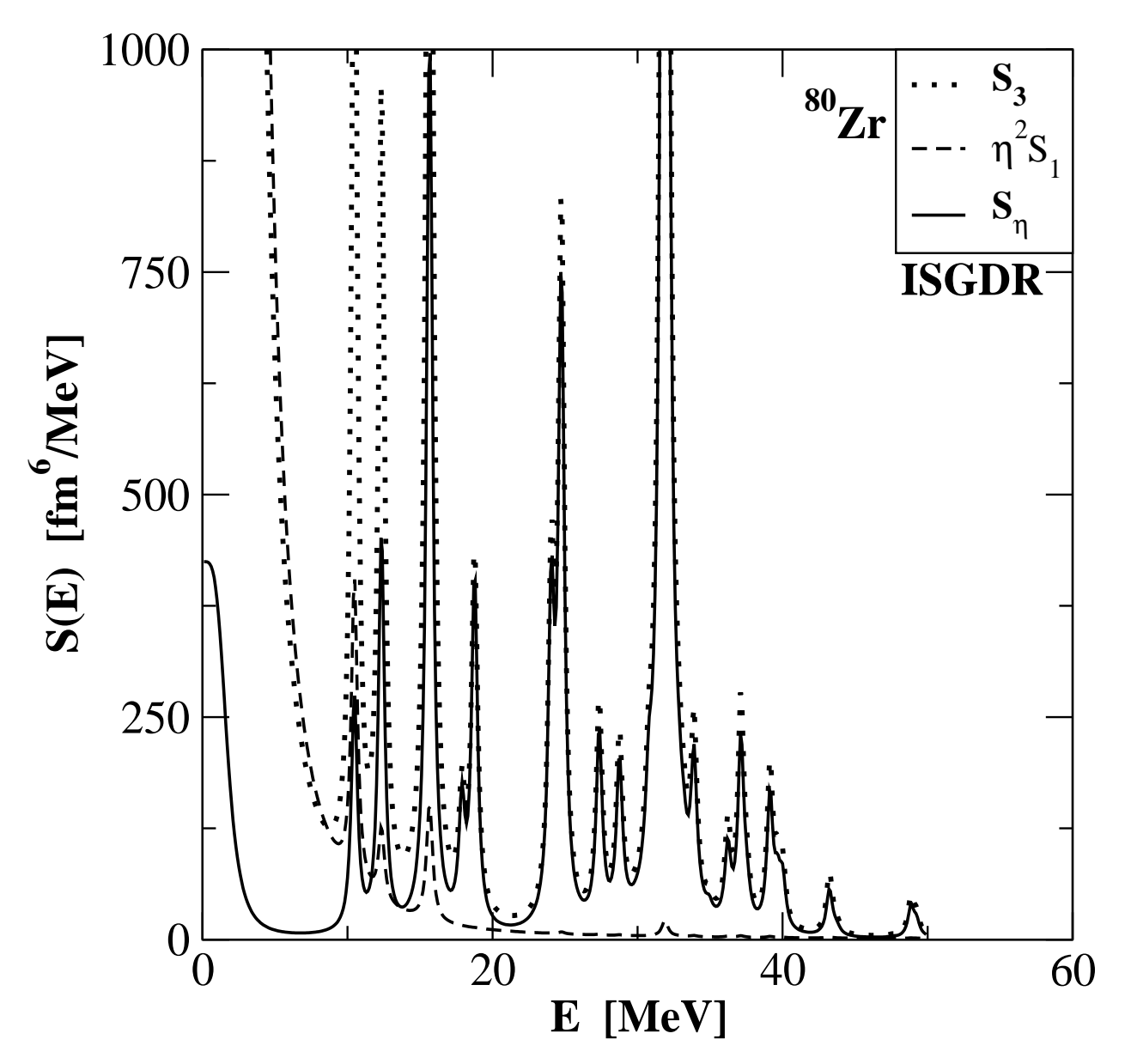


Fig. 12c

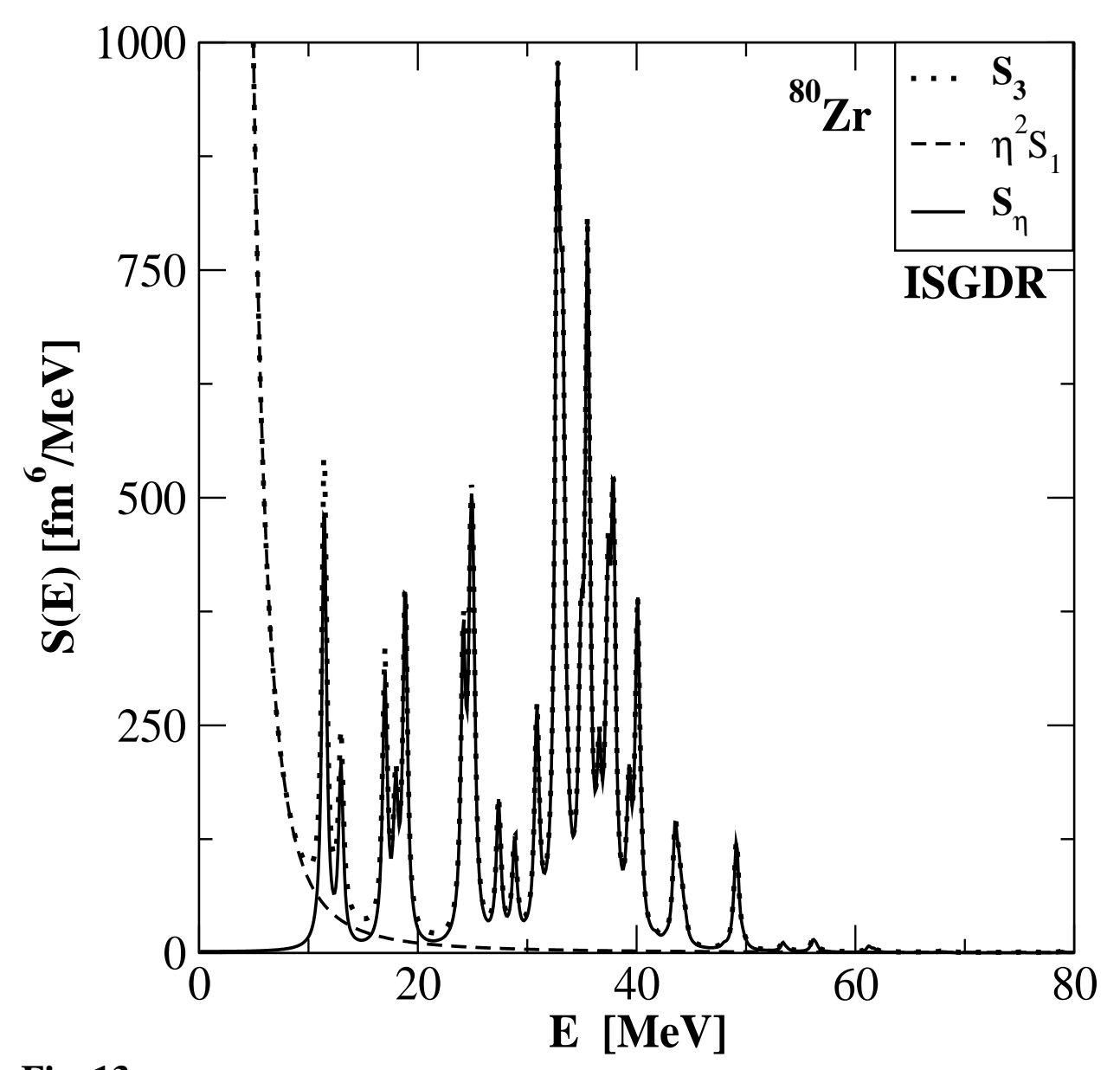


Fig. 13a

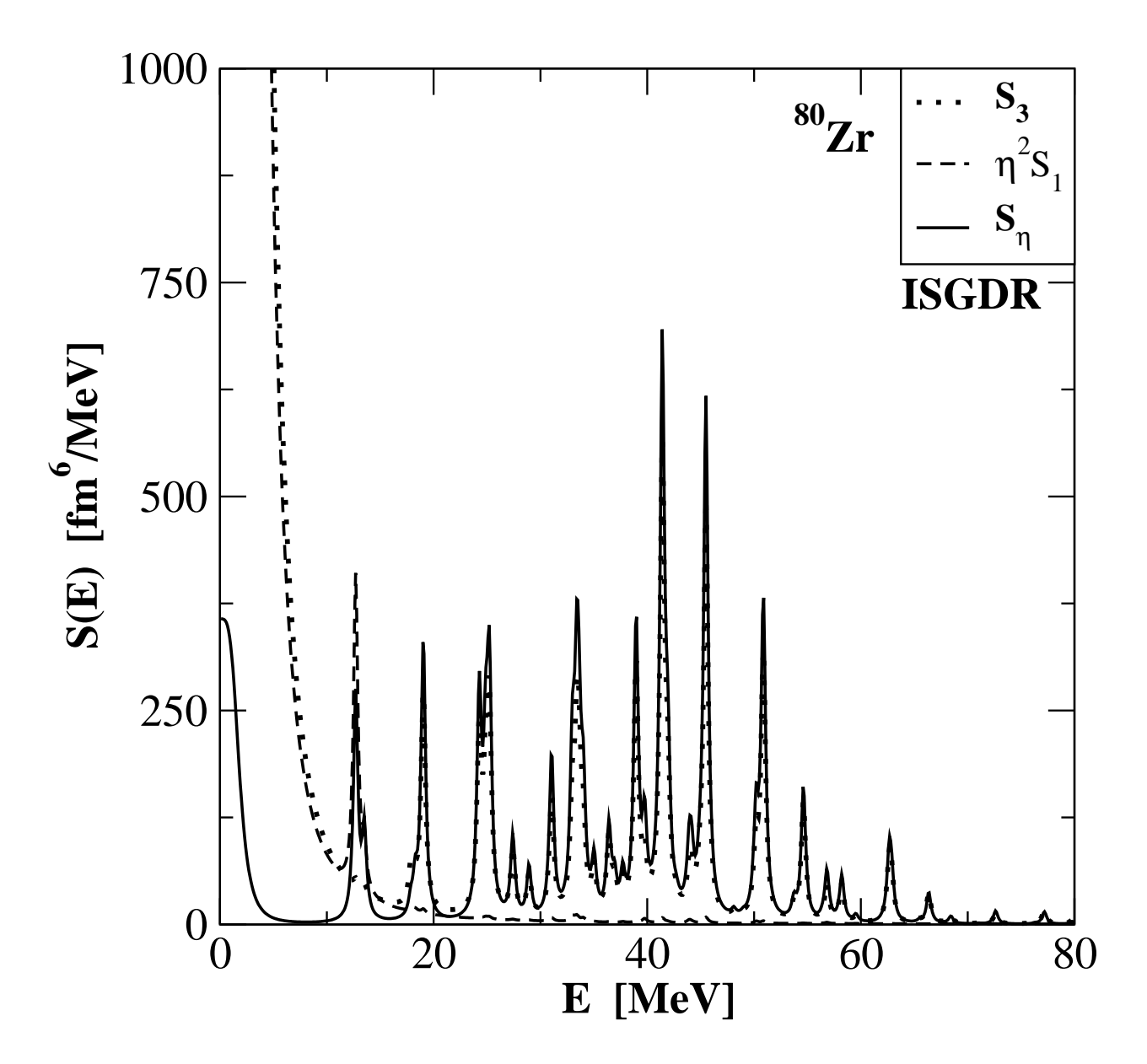
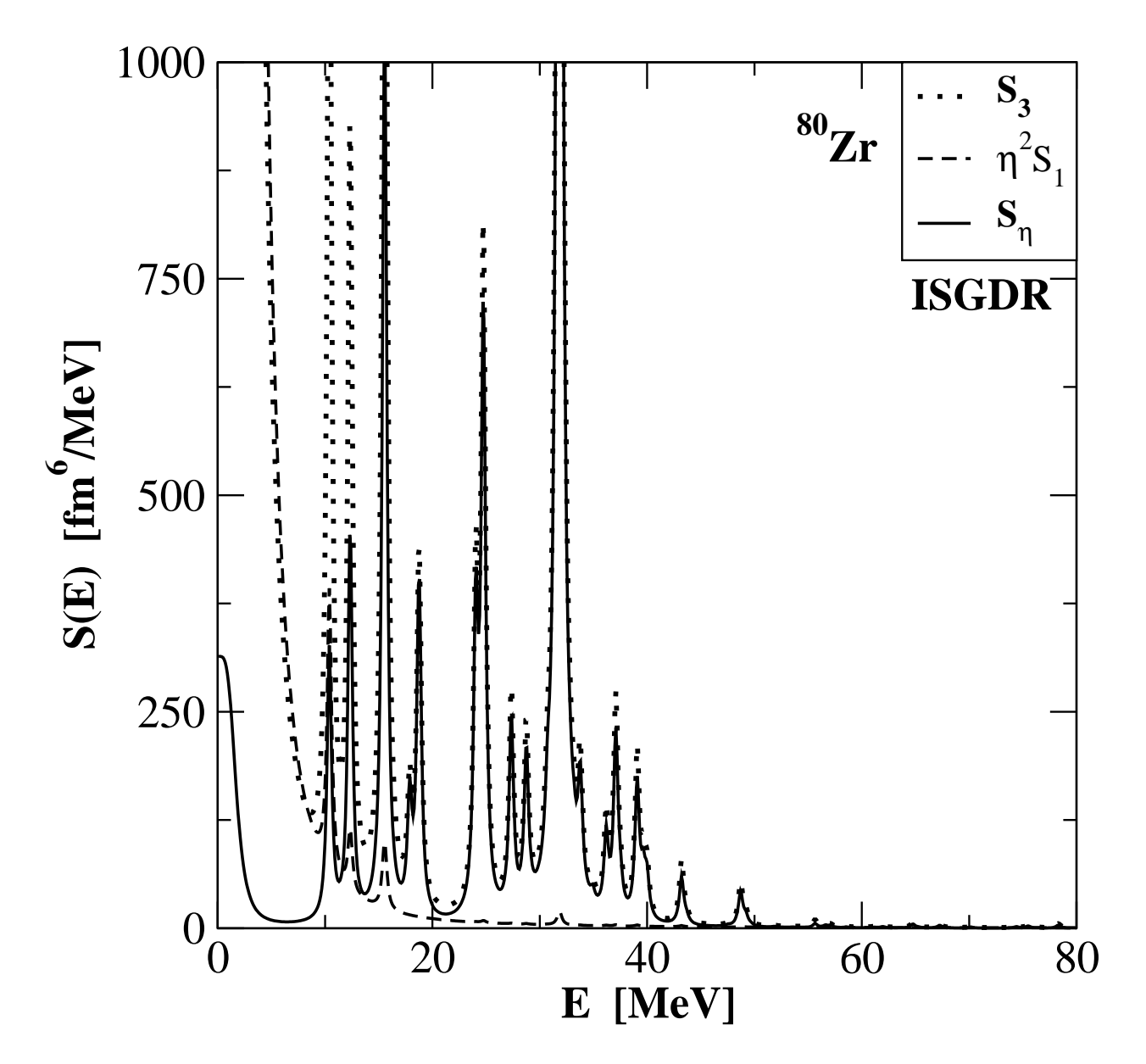


Fig. 13b



**Fig. 13c**